

# COMBSS: Best Subset Selection via Continuous Optimization

Sarat Moka<sup>1,\*</sup>, Benoit Liquet<sup>1</sup>, Houying Zhu<sup>1</sup>, and Samuel Muller<sup>1,2</sup>

<sup>1</sup> School of Mathematical and Physical Sciences, Macquarie University, Sydney, Australia

<sup>2</sup> School of Mathematics and Statistics, University of Sydney, Sydney, Australia

\* Corresponding author: sarat.moka@mq.edu.au

May 6, 2022

## Abstract

We consider the problem of best subset selection in linear regression, where the goal is to find for every model size  $k$ , that subset of  $k$  features that best fits the response. This is particularly challenging when the total available number of features is very large compared to the number of data samples. We propose COMBSS, a novel continuous optimization based method that directly solves the best subset selection problem in linear regression. COMBSS turns out to be very fast, potentially making best subset selection possible when the number of features is well in excess of thousands. Simulation results are presented to highlight the performance of COMBSS in comparison to existing popular non exhaustive methods such as Forward Stepwise and the Lasso, as well as for exhaustive methods such as Mixed-Integer Optimization. Because of the outstanding overall performance, framing the best subset selection challenge as a continuous optimization problem opens new research directions for feature extraction for a large variety of regression models.

## 1 Introduction

Recent rapid developments in information technology have enabled the collection of high-dimensional complex data, including in engineering, economics, finance, biology, and health sciences [8]. High-dimensional means that the number of features is large and often far higher than the number of collected data samples. In many of these applications, it is desirable to find a small best subset of predictors so that the resulting model has desirable prediction accuracy [9, 21]. In this article, we recast the challenge of best subset selection in linear regression as a continuous optimization problem. We show that this reframing has enormous potential and substantially advances research into larger dimensional and exhaustive feature selection in regression, making available best subset selection when  $p$  is well in excess of 1000s.

Consider the linear regression model  $\mathbf{y} = X\boldsymbol{\beta} + \boldsymbol{\epsilon}$ , where  $\mathbf{y} = (y_1, \dots, y_n)^\top$  is an  $n$ -dimensional known response vector,  $X$  is a known design matrix of dimension  $n \times p$  with  $x_{i,j}$  indicating the  $i$ -th observation of the  $j$ -th explanatory variable,  $\boldsymbol{\beta} = (\beta_1, \dots, \beta_p)^\top$  is the  $p$ -dimensional vector

of unknown regression coefficients, and  $\boldsymbol{\epsilon} = (\epsilon_1, \dots, \epsilon_n)^\top$  is a vector of unknown errors, unless otherwise specified, assumed to be independent and identically distributed (iid).

Best subset selection is a classical problem that aims to solve,

$$\underset{\boldsymbol{\beta} \in \mathbb{R}^p}{\text{minimize}} \quad \frac{1}{n} \|\mathbf{y} - X\boldsymbol{\beta}\|_2^2 \quad \text{subject to } \|\boldsymbol{\beta}\|_0 = k, \quad (1)$$

for a given  $k$ , where  $\|\cdot\|_2$  is the usual  $\mathcal{L}_2$ -norm, and  $\|\boldsymbol{\beta}\|_0 = \sum_{j=1}^p I(\beta_j \neq 0)$ , the number of non-zero elements in  $\boldsymbol{\beta}$ . For ease of reading, in this article, we assume that all columns of  $X$  are subject to selection.

In many practical settings, it is assumed that only a small number of explanatory variables contribute in the data generating model to the response, say there are at most  $q \ll \min(n, p)$  non-zero regression coefficients. Thus, best subset selection aims to solve (1) for every  $k \leq q$  to select indices of the non-zero regression coefficients while taking all other regression coefficients to be zero.

When the additional aim is to select the best model among all the best subset models of size  $k = 0, \dots, q$ , this is often achieved by using some performance measure such as criteria that minimize the *prediction error* or *information criteria*. Examples for the latter include the AIC [1] and BIC [24], we refer to [22] for a review on information criteria in linear regression.

Exact methods for solving (1) are typically executed by first writing solutions for low-dimensional problems and then selecting the best subset solution over these low dimensional problems. To see this, for any binary vector  $\mathbf{s} = (s_1, \dots, s_p)^\top \in \{0, 1\}^p$ , let  $X_{[\mathbf{s}]}$  be the matrix of size  $n \times |\mathbf{s}|$  created by keeping only columns  $j$  of  $X$  for which  $s_j = 1$ , where  $j = 1, \dots, p$ . Then, for every  $k \leq q$ , in exact best subset selection, the optimal  $\mathbf{s}$  can be found by solving the problem,

$$\underset{\mathbf{s} \in \{0, 1\}^p}{\text{minimize}} \quad \frac{1}{n} \|\mathbf{y} - X_{[\mathbf{s}]} \widehat{\boldsymbol{\beta}}_{[\mathbf{s}]}\|_2^2 \quad \text{subject to } |\mathbf{s}| = k, \quad (2)$$

where  $\widehat{\boldsymbol{\beta}}_{[\mathbf{s}]}$  is the low-dimensional least squares estimate of elements of  $\boldsymbol{\beta}$  with indices corresponding to non-zero elements of  $\mathbf{s}$ , i.e.

$$\widehat{\boldsymbol{\beta}}_{[\mathbf{s}]} = (X_{[\mathbf{s}]}^\top X_{[\mathbf{s}]})^{-1} X_{[\mathbf{s}]}^\top \mathbf{y}, \quad (3)$$

whenever the matrix inverse  $(X_{[\mathbf{s}]}^\top X_{[\mathbf{s}]})^{-1}$  exists, which is possible when the matrix  $X_{[\mathbf{s}]}^\top X_{[\mathbf{s}]}$  is of full rank  $k$ . The solution of (2) is identical to the solution of (1), because  $\widehat{\boldsymbol{\beta}}_{[\mathbf{s}]}$  is the least squares solution when constrained so that  $I(\beta_j \neq 0) = s_j$  for all  $j = 1, \dots, p$ .

It is well-known that solving the exact optimization problem in (1) is NP-hard [23] in general. For instance, a popular exact method called *leaps and bounds* [10] is practically useful only for values of  $p$  smaller than 30, as for example is the case when using the R package *leaps* [19] or *mpIot* [27].

In this paper, we design COMBSS, a novel *continuous optimization method for best subset selection*. To the best of our knowledge, COMBSS is the first attempt to exploit continuous optimization for directly solving the best subset selection problem.

In a nutshell, COMBSS can be described as follows: Instead of the binary vector space  $\{0, 1\}^p$  as in the exact methods, we consider the hyper-cube  $[0, 1]^p$  and define for each  $\mathbf{t} \in [0, 1]^p$  a new estimate

$\tilde{\beta}_t$  so that we have the following well-defined continuous extension of the exact problem (2):

$$\underset{t \in [0,1]^p}{\text{minimize}} \quad \frac{1}{n} \|\mathbf{y} - X_t \tilde{\beta}_t\|_2^2 + \lambda \sum_{j=1}^p t_j, \quad (4)$$

where  $X_t$  is obtained from  $X$  by multiplying the  $j$ -th column of  $X$  by  $t_j$  for all  $j = 1, \dots, p$ , and the tuning parameter  $\lambda$  controls the sparsity of the solution obtained, analogous to selecting the best  $k \leq q$  in the exact optimization.

Although, COMBSS aims to solve the best subset problem, an important property is that it has no discrete constraints, unlike the exact optimization problem (2). As a consequence, COMBSS can take advantage of standard continuous optimization methods, such as the basic gradient descent method, by starting at an interior point on the hypercube  $[0, 1]^p$  and iteratively moving towards a corner that minimizes the objective function. In the implementation, we move the box constrained problem (4) to an equivalent unconstrained problem so that the gradient descent method can run without any boundary issues.

The following list provides some key features of COMBSS that make it a novel, fast, and efficient best subsets approach:

- Unlike in the exact method, where  $X_{[s]}$  is constructed by removing columns from the design matrix  $X$  (and hence  $X_{[s]}$  and  $X$  are of different sizes),  $X_t$  in COMBSS is constructed by multiplying the  $j$ -th column of  $X$  by  $t_j$  for every  $j$ . Thus, both  $X_t$  and  $X$  are of the same size.

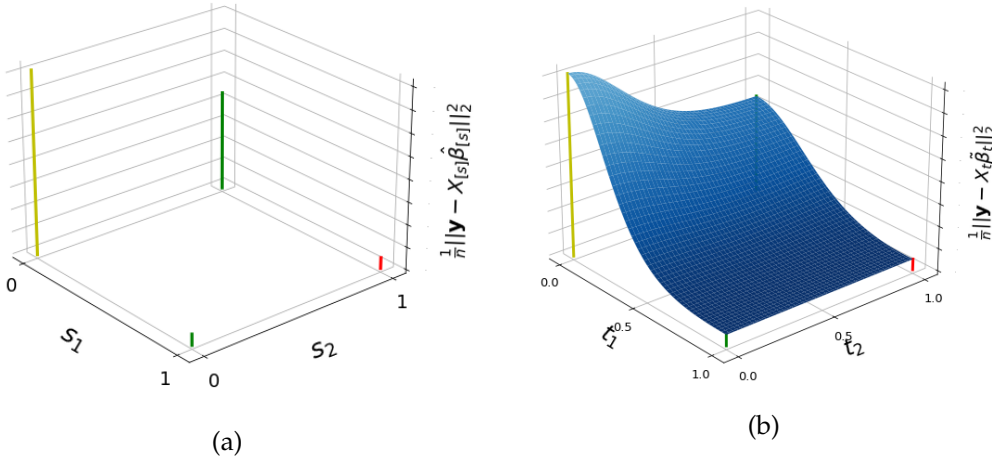


Figure 1:  $\frac{1}{n} \|\mathbf{y} - X_{[s]} \hat{\beta}_{[s]}\|_2^2$  vs  $\frac{1}{n} \|\mathbf{y} - X_t \tilde{\beta}_t\|_2^2$  for the data used later in Example 1. Intuitively, if we roll a ball (i.e., running a gradient descent algorithm) on the surface of  $\frac{1}{n} \|\mathbf{y} - X_t \tilde{\beta}_t\|_2^2$  shown in Panel (b), it will reach to the minimum point, which is  $(1, 1)^\top$  for this example. By adding the penalty  $\lambda \sum_{j=1}^p t_j$  and changing  $\lambda$ , we can control the path of the ball so that it reaches a sparse  $t$ .

- Our construction of the new coefficient estimator  $\tilde{\beta}_t$  guarantees that at the corner points  $s$  of the hyper-cube,  $\|\mathbf{y} - X_s \tilde{\beta}_s\|_2 = \|\mathbf{y} - X_{[s]} \hat{\beta}_{[s]}\|_2$ , where  $\hat{\beta}_{[s]}$  exists, while making sure that the new objective function  $\frac{1}{n} \|\mathbf{y} - X_t \tilde{\beta}_t\|_2^2$  has smooth transition from one corner to another. For instance, see Figure 1 for an illustration.

- By increasing the value of  $\lambda$ , we can increase the sparsity of the solution of the optimization problem (4), because the penalty  $\lambda \sum_{j=1}^p t_j$  encourages sparsity in  $\mathbf{t}$ .
- Solving the best subset selection problem using an exhaustive search is currently infeasible when  $p$  is of a moderate size as the number of visited models increases exponentially. However, COMBSS enables us to visit this huge space by exploiting the continuity of the objective function. Thus, a gradient descent algorithm can converge in a few iterations to the solution.
- We show that during the execution of the gradient descent, if some  $t_j$  converges to a small value close to zero, the algorithm pushes  $t_j$  to be zero. We also show that once  $t_j$  becomes zero, the corresponding  $j$ -th column of the design matrix ceases to play a role in the gradient descent updates that follow. As a consequence of these two observations, we propose some algorithmic improvements that provide further substantial speed improvements to COMBSS.

We provide sample code that makes available COMBSS in Python and R at

- <https://github.com/saratmoka/COMBSS-Python-VIGNETTE> and
- <https://github.com/benoit-liquet/COMBSS-R-VIGNETTE>, respectively.

The code includes examples where  $p$  is as large as of order 10,000. This code further allows to replicate our empirical research in this article. In ongoing technological development, we are currently working towards adding further functionality to this sample code. We aim to release COMBSS as an R software package on CRAN and as a Python software package on PyPI as soon as possible. We will update the above links accordingly when that work is finalised and will also add references to follow-up papers, where more detail is given on the computational and other aspects of COMBSS.

*Popular Existing Methods:* Even though the best subset selection problem is classical, for many years, it is generally believed that the problem is not feasible for large values of  $p$ . Relatively recent work [4] formulates (1) as a *mixed integer optimization* (MIO) problem and demonstrates that the best subset selection problem can be solved for much larger  $p$  using modern MIO solvers such as in the commercial software *Gurobi* [12], which is not freely available (except for an initial short period). In particular, the best subset selection problem is reformulated as the following MIO problem, containing both continuous constraints and discrete constraints:

$$\begin{aligned}
& \underset{\beta, \mathbf{z} \in \mathbb{R}^p}{\text{minimize}} && \frac{1}{n} \|\mathbf{y} - X\beta\|_2^2 \\
& \text{subject to} && -b z_j \leq \beta_j \leq b z_j, \quad j = 1, \dots, p, \\
& && z_j \in \{0, 1\}, \quad j = 1, \dots, p, \\
& && \sum_{j=1}^p z_j = k,
\end{aligned} \tag{5}$$

where  $b$  is a constant such that if  $\beta^*$  minimizes (5), then  $|\beta_j^*| \leq b$  for all  $j = 1, \dots, p$ .

Despite the fact that the MIO approach directly aims to solve the best subset selection problem and is faster than the exact method for larger values of  $p$ , its implementation via *Gurobi* is significantly

slow from a practical point of view. As a result, some of the indirect methods, such as *Forward Stepwise selection* and the *least absolute shrinkage and selection operator* (Lasso) and their variants, are still very common in practice. *Forward Stepwise selection* follows a greedy approach which, starting with an empty model (or intercept only model), iteratively adds the variable that is best suited [7, 16]. On the other hand, instead of solving the highly non-convex best subset selection problem, Lasso introduced in [29] solves a convex relaxation of it by replacing the (discrete)  $\mathcal{L}_0$  norm  $\|\beta\|_0$  in (1) with the  $\mathcal{L}_1$  norm  $\|\beta\|_1$ . Due to this clever relaxation, Lasso is a convex optimization problem. Thus, it is fast (and much faster than the MIO solvers). However, it is known that Lasso solutions are lacking of crucial statistical quality [25] and do not normally lead to a best subset [15, 31] solution.

The rest of the paper is organized as follows: In Section 2, we describe the mathematical framework required for stating the proposed optimization method COMBSS. In Section 3, we first establish the continuity of the objective functions involved in COMBSS, and then we derive expressions for their gradients. These gradients are later exploited for conducting continuous optimization. A detailed algorithm for COMBSS is given in Section 4. In Section 5, we discuss how to choose the tuning parameters that control the surface shape of the objective functions and the sparsity of the solutions obtained. Section 6 provides steps for efficient implementation of COMBSS using some linear algebra techniques. In Section 7 we present a simulation study to show the good behaviour and the performance of COMBSS compared to traditional methods in low and high dimensional context. We conclude the paper in Section 8 with a discussion on possible future improvements for COMBSS.

## 2 Continuous Extension of the Best Subset Selection Problem

In this section, we provide the mathematical setup for COMBSS, which solves a continuous extension of the exact best subset selection optimization problem (2).

For  $\mathbf{t} = (t_1, \dots, t_p)^\top \in [0, 1]^p$  define  $T_{\mathbf{t}} = \text{Diag}(\mathbf{t})$ , the diagonal matrix with the diagonal elements being  $t_1, \dots, t_p$ , and

$$X_{\mathbf{t}} = XT_{\mathbf{t}}.$$

For a fixed constant  $\delta > 0$ , define

$$L_{\mathbf{t}} = L_{\mathbf{t}}(\delta) = \frac{1}{n} \left[ X_{\mathbf{t}}^\top X_{\mathbf{t}} + \delta (I - T_{\mathbf{t}}^2) \right] \quad (6)$$

and we suppress  $\delta$  for ease of reading. Intuitively,  $L_{\mathbf{t}}$  can be seen as a ‘convex combination’ of the matrices  $(X^\top X)/n$  and  $\delta I/n$ , because  $X_{\mathbf{t}}^\top X_{\mathbf{t}} = T_{\mathbf{t}} X^\top X T_{\mathbf{t}}$  and thus

$$L_{\mathbf{t}} = T_{\mathbf{t}} \left( \frac{X^\top X}{n} \right) T_{\mathbf{t}} + (I - T_{\mathbf{t}}) \left( \frac{\delta}{n} I \right) (I - T_{\mathbf{t}}).$$

Now let

$$\tilde{\beta}_{\mathbf{t}} := L_{\mathbf{t}}^+ \left( \frac{X_{\mathbf{t}}^\top \mathbf{y}}{n} \right), \quad \mathbf{t} \in [0, 1]^p, \quad (7)$$

where  $L_{\mathbf{t}}^+$  is the pseudo-inverse (or, the Moore-Penrose inverse) of  $L_{\mathbf{t}}$ . We need  $L_{\mathbf{t}}^+$  in (7) so that  $\tilde{\beta}_{\mathbf{t}}$  is defined for all  $\mathbf{t} \in [0, 1]^p$ . However, from the way we conduct optimization, we need to compute  $\tilde{\beta}_{\mathbf{t}}$  only for  $\mathbf{t} \in [0, 1]^p$ . We later show in Theorem 1 that for all  $\mathbf{t} \in [0, 1]^p$ ,  $L_{\mathbf{t}}$  is invertible and thus in the implementation of COMBSS,  $\tilde{\beta}_{\mathbf{t}}$  always takes the form  $\tilde{\beta}_{\mathbf{t}} = L_{\mathbf{t}}^{-1} (X_{\mathbf{t}}^{\top} \mathbf{y}/n)$ , eliminating the need to compute any computationally expensive pseudo-inverse.

With the support of these observations, the following is an immediate well defined generalization of best subset problem (1):

$$\underset{\mathbf{t} \in [0, 1]^p}{\text{minimize}} \quad \frac{1}{n} \|\mathbf{y} - X_{\mathbf{t}} \tilde{\beta}_{\mathbf{t}}\|_2^2 \quad \text{subject to} \quad \sum_{j=1}^p t_j \leq q. \quad (8)$$

The optimization problem (8) is a constrained problem. Instead of solving this, by defining a Lagrangian function

$$f_{\lambda}(\mathbf{t}) = \frac{1}{n} \|\mathbf{y} - X_{\mathbf{t}} \tilde{\beta}_{\mathbf{t}}\|_2^2 + \lambda \sum_{j=1}^p t_j, \quad (9)$$

for a tunable parameter  $\lambda > 0$ , we aim to solve instead

$$\underset{\mathbf{t} \in [0, 1]^p}{\text{minimize}} \quad f_{\lambda}(\mathbf{t}). \quad (10)$$

We can reformulate the box constrained problem (10) into an equivalent unconstrained problem by considering the mapping  $\mathbf{t} = \mathbf{t}(\mathbf{w})$  given by

$$t_j(w_j) = 1 - \exp(-w_j^2), \quad j = 1, \dots, p, \quad (11)$$

and then rewriting (10) as,

$$\underset{\mathbf{w} \in \mathbb{R}^p}{\text{minimize}} \quad f_{\lambda}(\mathbf{t}(\mathbf{w})). \quad (12)$$

The unconstrained optimization problem (12) is equivalent to the box constrained problem (10), because for any  $u, v \in \mathbb{R}$ ,

$$1 - \exp(-u^2) < 1 - \exp(-v^2) \quad \text{if and only if} \quad u^2 < v^2.$$

In summary, by defining,

$$g_{\lambda}(\mathbf{w}) = f_{\lambda}(\mathbf{t}(\mathbf{w})), \quad (13)$$

we solve,

$$\underset{\mathbf{w} \in \mathbb{R}^p}{\text{minimize}} \quad g_{\lambda}(\mathbf{w}), \quad (14)$$

via some continuous optimization method, such as a gradient descent method.

We recall that our ultimate goal is to find a solution of the best subset selection problem (2). Suppose that  $\mathbf{w}^*$  denotes the solution of (14) obtained by a gradient descent method. Then, the corresponding solution  $\mathbf{t}^*$  of (10) is obtained through the mapping (11). Further using this  $\mathbf{t}^*$ , we select an appropriate binary vector as a solution to (2); see Section 4 for complete details.

The following example shows the surface plots of the objective functions  $f_{\lambda}(\mathbf{t})$  and  $g_{\lambda}(\mathbf{w})$  for a simple case.

**Example 1.** We choose  $p = 2$  and  $n = 100$ , and generate each row of  $X$  from a multivariate Gaussian with mean  $\mu_x$  and covariance  $\Sigma_x$  given by

$$\mu_x = \begin{bmatrix} 1 \\ 1 \end{bmatrix} \quad \text{and} \quad \Sigma_x = \begin{bmatrix} 3 & 1 \\ 1 & 2 \end{bmatrix}.$$

The noise  $\epsilon$  is generated from a standard normal and the true model has coefficient vector  $\beta = (2, 0)^\top$ . Suppose  $k = 1$  in the best subset selection problem (1). Since  $p$  is small, we can easily solve the exact problem (2) to find its optimal solution  $s^* = (1, 0)^\top$ . Refer to Figure 2 to see the surface plots of  $f_\lambda(\mathbf{t})$  and  $g_\lambda(\mathbf{w})$  for  $\lambda = 0$  and  $\lambda = 1.5$ . Observe that when  $\lambda$  is positive, the surface of  $f_\lambda(\mathbf{t})$  is exhibiting a downwards slope towards  $s^*$  from all the directions. Similarly, for positive  $\lambda$ , the surface of  $g_\lambda(\mathbf{w})$  is exhibiting a valley around the line  $w_2 = 0$ , and this helps the gradient descent algorithm to traverse towards optimal points  $(\pm\infty, 0)^\top$ .  $\square$

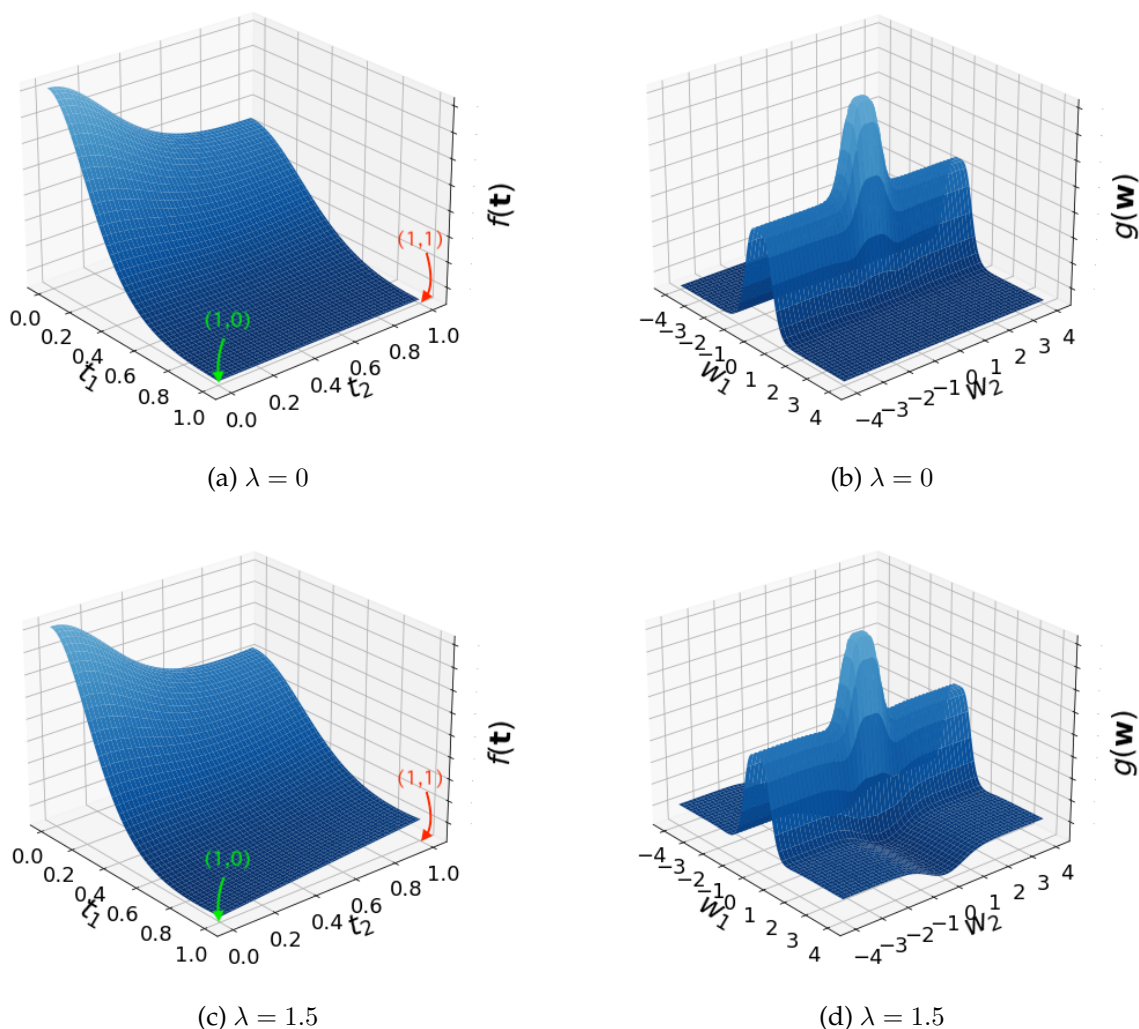


Figure 2: Surface plots of the objective functions  $f_\lambda(\mathbf{t})$  and  $g_\lambda(\mathbf{w})$  for  $\lambda = 0$  and  $\lambda = 1.5$ . To see the effect of changing  $\lambda$ , compare the values of  $f_\lambda(\mathbf{t})$  in Panel (a) and Panel (c) at  $\mathbf{t} = (1, 0)^\top$  and  $\mathbf{t} = (1, 1)^\top$ .

### 3 Continuity and Gradients of the Objective Function

In this section, we first prove that the objective function  $g_\lambda(\mathbf{w})$ , defined in (13), is continuous on  $\mathbb{R}^p$  and then we derive its gradients. En-route, we also establish the relationship between  $\widehat{\beta}_s$  and  $\widetilde{\beta}_t$  which are respectively defined by (3) and (7). This relationship is useful in understanding the relationship between our method COMBSS and the exact optimization (2). The detailed proofs of all the results in this section are available in Appendix A.

Our first result, Theorem 1, shows that for all  $\mathbf{t} \in [0, 1]^p$ , the matrix  $L_t$ , which is defined in (6), is symmetric positive definite and hence invertible.

**Theorem 1.** *For any  $\mathbf{t} \in [0, 1]^p$ ,  $L_t$  is symmetric and positive-definite and*

$$\widetilde{\beta}_t = L_t^{-1} \left( \frac{X_t^\top \mathbf{y}}{n} \right).$$

Recall that  $\widehat{\beta}_{[s]}$  exists only on some corner points,  $\mathbf{s}$ , of the hyper-cube  $[0, 1]^p$ , where the matrix  $X_{[s]}^\top X_{[s]}$  is invertible. Theorem 2 establishes a relationship between  $\widetilde{\beta}_s$  and  $\widehat{\beta}_{[s]}$  at these corner points  $\mathbf{s} \in \{0, 1\}^p$ .

**Theorem 2.** *For any point  $\mathbf{s} \in \{0, 1\}^p$ ,  $\widehat{\beta}_{[s]}$  exists if and only if  $L_s$  is invertible and in that case,*

$$X_{[s]} \widehat{\beta}_{[s]} = X_s \widetilde{\beta}_s.$$

As an immediate result of Theorem 2, we have

$$f_\lambda(\mathbf{s}) = \frac{1}{n} \|\mathbf{y} - X_{[s]} \widehat{\beta}_{[s]}\|_2^2 + \lambda |\mathbf{s}|,$$

whenever  $\widehat{\beta}_{[s]}$  exists. That is, the objective function of the exact optimization problem (2) is identical to the objective function of its extended optimization problem (8).

Our next result, Theorem 3, shows that  $f_\lambda(\mathbf{t})$  is a continuous function on  $[0, 1]^p$ .

**Theorem 3.** *The function  $f_\lambda(\mathbf{t})$  defined in (9) is continuous over  $[0, 1]^p$  in the sense that for any sequence  $\mathbf{t}^{(1)}, \mathbf{t}^{(2)}, \dots \in [0, 1]^p$  converging to  $\mathbf{t} \in [0, 1]^p$ , the limit  $\lim_{l \rightarrow \infty} f_\lambda(\mathbf{t}^{(l)})$  exists and*

$$f_\lambda(\mathbf{t}) = \lim_{l \rightarrow \infty} f_\lambda(\mathbf{t}^{(l)}).$$

The next result, Corollary 1, establishes the continuity of  $g_\lambda$  on  $\mathbb{R}^p$ . This is a simple consequence of Theorem 3, because from the definition (13),  $g_\lambda(\mathbf{w}) = f(\mathbf{t}(\mathbf{w}))$  with  $\mathbf{t}(\mathbf{w}) = \mathbf{1} - \exp(-\mathbf{w} \odot \mathbf{w})$ , here (and afterwards)  $\mathbf{1}$  denotes a vector of all 1's of appropriate dimension,  $\odot$  denotes the element-wise product of two vectors, and the function  $\exp$  is applied element-wise.

**Corollary 1.** *The objective function  $g_\lambda(\mathbf{w})$  is continuous at every point  $\mathbf{w} \in \mathbb{R}^p$ .*

As mentioned earlier, COMBSS uses a gradient descent method to solve the problem (14). Towards that we need to obtain the gradients of  $g_\lambda(\mathbf{w})$ . Theorem 4 provides an expression of the gradient  $\nabla g_\lambda(\mathbf{w})$  for every  $\mathbf{w} \in \mathbb{R}^p$ .

**Theorem 4.** For every  $\mathbf{w} \in \mathbb{R}^p$ , with  $\mathbf{t} = \mathbf{t}(\mathbf{w})$  is given by (11),

$$\nabla f_\lambda(\mathbf{t}) = \boldsymbol{\zeta}_t + \lambda \mathbf{1}, \quad \mathbf{t} \in (0, 1)^p,$$

and

$$\nabla g_\lambda(\mathbf{w}) = (\boldsymbol{\zeta}_t + \lambda \mathbf{1}) \odot (2\mathbf{w} \odot \exp(-\mathbf{w} \odot \mathbf{w})), \quad \mathbf{w} \in \mathbb{R}^p,$$

where

$$\boldsymbol{\zeta}_t = 2 \left( \tilde{\boldsymbol{\beta}}_t \odot (\mathbf{a}_t - \mathbf{d}_t) \right) - 2 (\mathbf{b}_t \odot \mathbf{c}_t), \quad (15)$$

with

$$\begin{aligned} \mathbf{a}_t &= \left( \frac{X^\top X}{n} \right) (\mathbf{t} \odot \tilde{\boldsymbol{\beta}}_t) - \left( \frac{X^\top \mathbf{y}}{n} \right), \\ \mathbf{b}_t &= \mathbf{a}_t - \frac{\delta}{n} (\mathbf{t} \odot \tilde{\boldsymbol{\beta}}_t), \\ \mathbf{c}_t &= L_t^{-1} (\mathbf{t} \odot \mathbf{a}_t), \quad \text{and} \\ \mathbf{d}_t &= \left( \frac{X^\top X}{n} - \frac{\delta}{n} I \right) (\mathbf{t} \odot \mathbf{c}_t). \end{aligned}$$

## 4 The COMBSS Algorithm

In this section, we state the pseudocode for COMBSS and provide a discussion on how to execute the algorithm.

Overall, Algorithm 1 consists of two stages. First stage, Step 1, calls a gradient descent method of choice to obtain a solution  $\mathbf{w}^*$  of the unconstrained optimization problem (14). In the second stage, Steps 2 to 5, a solution  $\mathbf{t}^*$  of the box constrained optimization problem (10) is obtained from  $\mathbf{w}^*$  using the map  $\mathbf{t}(\mathbf{w}) = 1 - \exp(-\mathbf{w} \odot \mathbf{w})$  and then mapping small (respectively, large) values of  $\mathbf{t}^*$  to 0 (respectively, 1) (shown in Step 4), a solution of the discrete constrained best subset selection problem (2) is obtained.

---

### Algorithm 1: COMBSS

---

**Input:** Dataset  $(X, \mathbf{y})$   
Tuning parameters  $\delta$  and  $\lambda$   
The initial vector  $\mathbf{w}^{(0)}$   
Threshold value  $\tau \in [0, 1]$   
Termination condition TermCond

**Output:** A binary vector  $\mathbf{s}$  as a solution to the optimization problem (2)

```

1  $\mathbf{w} \leftarrow \text{GradientDescent}(\mathbf{w}^{(0)}, \text{TermCond}, \nabla g_\lambda)$ 
2  $\mathbf{t} \leftarrow 1 - \exp(-\mathbf{w} \odot \mathbf{w})$ 
3 for  $j = 1, \dots, p$  do
4    $s_j = I(t_j > \tau)$ 
5 return  $\mathbf{s} = (s_1, \dots, s_p)^\top$ 

```

---

The subroutine `GradientDescent` ( $\mathbf{w}^{(0)}$ , `TermCond`,  $\nabla g_\lambda$ ) calls a gradient descent method for minimizing the objective function  $g_\lambda(\mathbf{w})$ , takes  $\mathbf{w}^{(0)}$  as the initial point for the gradient descent method, uses the gradient function  $\nabla g_\lambda$  for updating the vector  $\mathbf{w}$  in each iteration of the gradient descent method, and terminates to return the final value of  $\mathbf{w}$  when the given termination condition `TermCond` is satisfied. There are several well-known gradient descent methods in the literature. For the reader’s convenience, in Appendix B, we briefly review two such methods, namely, the *basic gradient descent* method and the *adaptive moment estimation* algorithm (simply known as Adam optimizer). The latter method is popular in deep learning for solving highly non-convex optimization problems.

There are few things to keep in mind while selecting the initial point  $\mathbf{w}^{(0)}$  for the gradient descent. Observe from Theorem 4 that, for any  $j = 1, \dots, p$ ,

- $t_j(w_j) = 0$  if and only if  $w_j = 0$ , and
- $\frac{\partial g_\lambda(\mathbf{w})}{\partial w_j} = 0$  if  $w_j = 0$ .

Thus, if we start a gradient descent algorithm with  $w_j^{(0)} = 0$  for some  $j$ , both  $w_j$  and  $t_j$  can continue to take 0 forever. As a result, we might not learn the optimal value for  $w_j$  (or, equivalently for  $t_j$ ). Thus, it is important to select  $w_j^{(0)}$  away from 0 for all  $j = 1, \dots, p$ . In our simulation, we select  $\mathbf{w}_0$  such that  $\mathbf{t}(\mathbf{w}_0) = (1/2, \dots, 1/2)^\top$ , the mid-point on the hyper cube  $[0, 1]^p$ . This is intuitively a good choice as it is at equal distance from all the corner points, of which one is the (unknown) target solution of the best subset selection problem. However, future work on how to better choose the initial vector  $\mathbf{w}_0$  may further improve the performance of COMBSS. In this paper, we do not further investigate this aspect.

The termination condition, `TermCond`, for the gradient descent method is a user choice depending on the computational budget. One trivial option is to terminate the algorithm after reaching a predefined maximum number of iterations or maximum allowed running time. Another option is to terminate when the change in  $\mathbf{w}$  (or, equivalently, in  $\mathbf{t}(\mathbf{w})$ ) is significantly small over a set of consecutive iterations. In our simulations, we take the latter approach by terminating when the max-norm

$$\|\mathbf{t}(\mathbf{w}^{(l)}) - \mathbf{t}(\mathbf{w}^{(l-1)})\|_\infty = \max_{j=1, \dots, p} |t_j(w_j^{(l)}) - t_j(w_j^{(l-1)})|$$

is smaller than a predefined error over a fixed number of consecutive iterations, where  $\mathbf{w}^{(l)}$  denotes the updated value of  $\mathbf{w}$  in the  $l$ -th iteration of the gradient descent method. This particular `TermCond` makes the algorithm robust by guaranteeing that further running of the algorithm possibly can bring only an insignificant change in every  $t_j$ .

Now, consider the last argument,  $\nabla g_\lambda$ , in the gradient descent method. From Theorem 4, observe that computing the gradient  $\nabla g_\lambda(\mathbf{w})$  involves finding the values of the expression of the form  $L_t^{-1}\mathbf{u}$  twice, first for computing  $\tilde{\beta}_t$  (using (7)) and then for computing the vector  $\mathbf{c}_t$  (defined in Theorem 4). Since  $L_t$  is a  $p \times p$  matrix, computing the matrix inversion  $L_t^{-1}$  can be problematic particularly in high-dimensional cases where  $p$  can be very large [11]. Since  $L_t^{-1}\mathbf{u}$  is the solution of the linear equation  $L_t\mathbf{z} = \mathbf{u}$ , in Section 6.1, we propose a conjugate gradient based approach for solving this linear equation efficiently without the need to compute  $L_t^{-1}$ .

Moreover, again from Theorem 4, notice that the gradient  $\nabla g_\lambda(\mathbf{w})$  depends on both the tuning parameters  $\delta$  and  $\lambda$ . Particularly,  $\delta$  is required for computing  $L_t$  and  $\lambda$  is used in the penalty term  $\lambda\|\mathbf{t}\|$  of the objective function. In Section 5 we provide more detail on the roles of these two parameters and instructions on how to choose them.

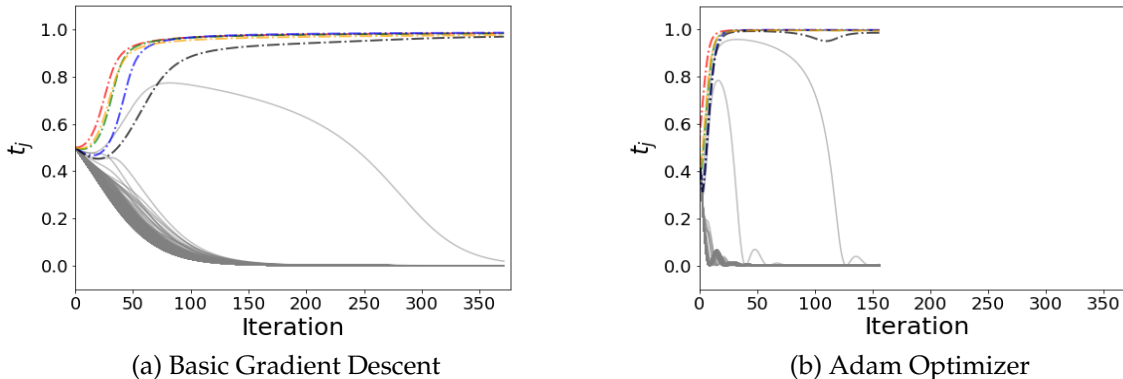


Figure 3: Convergence of  $\mathbf{t}$  for a dataset during the execution of the basic gradient descent (Panel (a)) and the Adam optimizer (Panel (b)). The dataset is generated using Beta-type 1 with  $k_0 = 5$ ,  $n = 100$ ,  $p = 1000$ ,  $\rho = 0.8$ , and  $\text{SNR} = 5$ ; see Section 7 for more details on data generation and selection of optimization parameters. For both the simulations,  $\lambda = 0.1$  and  $\delta = n$ ; see Section 5 for more discussion on how to choose  $\lambda$  and  $\delta$ . We terminated the gradient descent algorithms when  $\|\mathbf{t}(\mathbf{w}^{(l)}) - \mathbf{t}(\mathbf{w}^{(l-1)})\|_\infty \leq 0.001$  consecutively over 10 iterations. In both the figures, solid lines correspond to  $\beta_j = 0$  and remaining 5 curves (with line style  $-\cdot-$ ) correspond to  $\beta_j \neq 0$ .

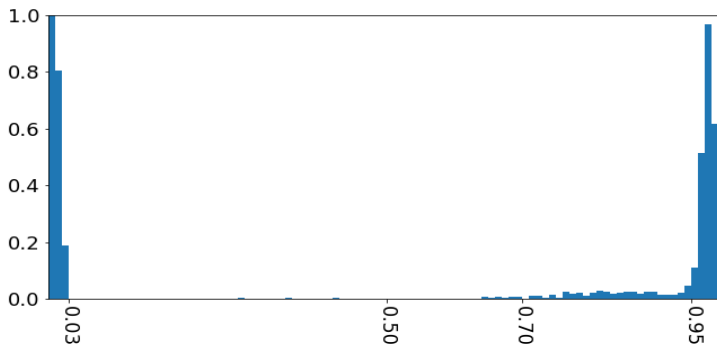


Figure 4: Histogram of the  $t_j$  values when COMBSS is executed on 500 independent datasets using the Adam optimizer. The parameters for data generation and simulation are the same as given in Figure 3. In the above histogram, each bin is of size 0.01 and the height of the  $i$ -th bar is the fraction of datasets for which the final output of the Adam optimizer has at least one  $t_j$  converged to a point in the  $i$ -th bin. Observe that since  $p = 1000$ , except for a tiny fraction of the datasets, each of the 1000  $t_j$ 's converges to a value close to either 0 or 1. This indicates that the output of COMBSS is not sensitive to the value of  $\tau$  if it is chosen away from the terminal values 0 and 1.

Figure 3 illustrates the convergence of  $t_j$  (within the gradient descent algorithm) using an example dataset for both the basic gradient descent method and the Adam optimizer. One useful observation from Figure 3 is that the Adam optimizer takes a smaller number of iterations for

convergence compared to the basic gradient descent method. This is expected because the Adam optimizer uses *momentum* updates which are not present in the basic gradient descent. In our simulations in Section 7, we use only the Adam optimizer.

Finally, the threshold parameter  $\tau \in (0, 1)$  at Step 4 of Algorithm 1 is useful for mapping all the insignificantly smaller  $t_j$ 's to 0 and all other  $t_j$ 's to 1. Due to the tolerance allowed by the termination condition TermCond, some  $w_j$ 's in the output of the gradient descent algorithm can be almost zero but not exactly zero, even though they are meant to converge to zero values. As a result, the corresponding  $t_j$ 's also take values close to zero but not exactly zero because of the mapping from  $\mathbf{w}$  to  $\mathbf{t}$  (see Step 2 on the algorithm). Therefore,  $\tau$  helps in mapping these insignificantly small values to zeros. Figure 4 illustrates that the final output of the algorithm is not sensitive to  $\tau$  as long as it is chosen slightly away from 0. For all our simulations in Section 7, we fix  $\tau = 0.5$ .

## 5 Roles of Tuning Parameters $\delta$ and $\lambda$

In this section, we provide insights on how the tuning parameters  $\delta$  and  $\lambda$  influence the objective function  $f_\lambda(\mathbf{t})$  (or, equivalently  $g_\lambda(\mathbf{w})$ ) and hence the convergence of the algorithm.

### 5.1 Controlling the Shape of $f_\lambda(\mathbf{t})$ through $\delta$

The normalized cost  $\|\mathbf{y} - X_{\mathbf{t}}\tilde{\beta}_{\mathbf{t}}\|_2^2/n$  provides an estimator of the error variance. For any fixed  $\mathbf{t}$ , we expect this variance (and hence  $f_\lambda(\mathbf{t})$ ) to be almost the same for all relatively large values of  $n$ , particularly, in situations where the errors  $\epsilon_i$ 's are iid. Clearly,  $f_\lambda(\mathbf{s})$  does not depend on  $\delta$  for all the corner points  $\mathbf{s} \in \{0, 1\}^p$  where  $L_{\mathbf{s}}$  is invertible, because at these corner points, from Theorem 2,  $X_{\mathbf{s}}\tilde{\beta}_{\mathbf{s}} = X_{[\mathbf{s}]}\hat{\beta}_{[\mathbf{s}]}$ , which is independent of  $\delta$ . We would like to have a similar behavior at all the interior points  $\mathbf{t} \in (0, 1)^p$  as well, so that for each  $\mathbf{t}$ , the function  $f_\lambda(\mathbf{t})$  is roughly the same for all large values of  $n$ . Such consistent behavior is helpful in guaranteeing that the convergence paths of the gradient descent method are approximately the same for all large values of  $n$ .

First reconsider the model given in Example 1. Figure 5 shows surface plots of  $f_\lambda(\mathbf{t})$  for different values of  $n$  and  $\delta$ . Here, there are two plots, i.e. Figure 5(a) and Figure 5(d), that correspond to  $\delta = n$ . In both these plots, we observe that the shape of the surface of  $f_\lambda(\mathbf{t})$  over  $[0, 1]^p$  is very similar.

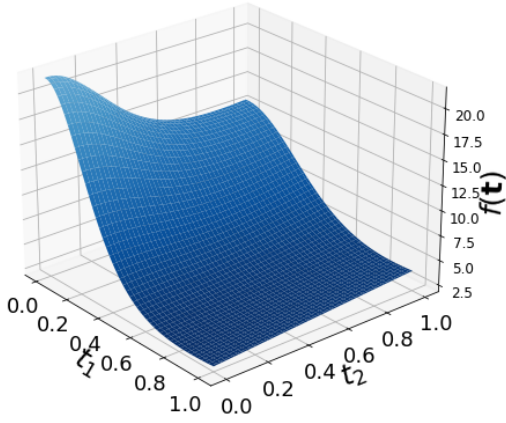
To make this more explicit, we now show that at every  $\mathbf{t}$  the function  $f_\lambda(\mathbf{t})$  takes almost the same value for all large  $n$  if we keep  $\delta = n$  under the assumption that the data samples are iid (this assumption simplifies the following discussion; however, the conclusion holds more generally).

Observe that

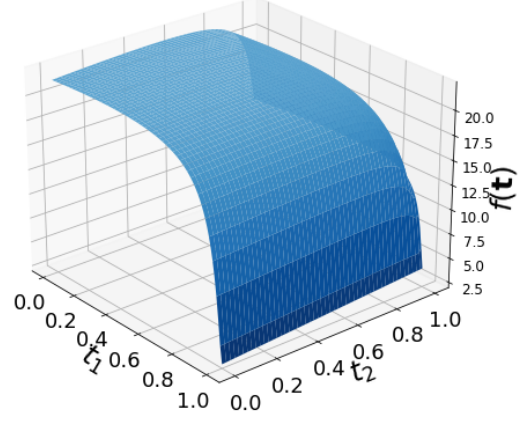
$$\frac{1}{n}\|\mathbf{y} - X_{\mathbf{t}}\tilde{\beta}_{\mathbf{t}}\|_2^2 = \frac{\mathbf{y}^\top \mathbf{y}}{n} - 2\gamma_{\mathbf{t}}^\top \left( \frac{X_{\mathbf{t}}^\top \mathbf{y}}{n} \right) + \gamma_{\mathbf{t}}^\top \left( \frac{X_{\mathbf{t}}^\top X_{\mathbf{t}}}{n} \right) \gamma_{\mathbf{t}},$$

where

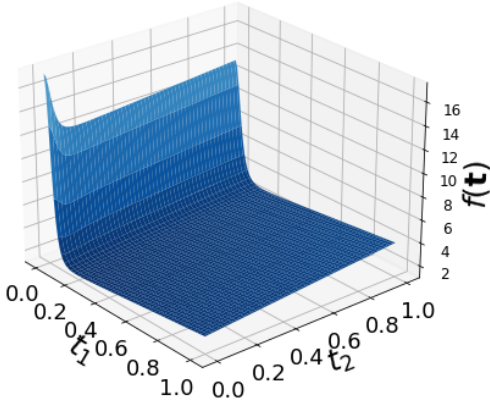
$$\gamma_{\mathbf{t}} = T_{\mathbf{t}} L_{\mathbf{t}}^{-1} T_{\mathbf{t}} \left( \frac{X_{\mathbf{t}}^\top \mathbf{y}}{n} \right).$$



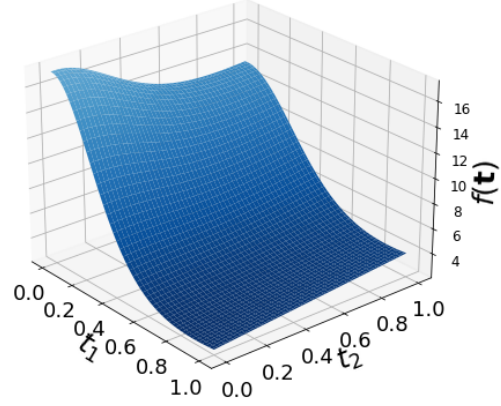
(a)  $n = 100$  and  $\delta = 100$



(b)  $n = 100$  and  $\delta = 10000$



(c)  $n = 10000$  and  $\delta = 100$



(d)  $n = 10000$  and  $\delta = 10000$

Figure 5: Illustration of effects of  $\delta$  on the objective function  $f_\lambda(\mathbf{t})$  with  $\lambda = 1.5$ . A dataset consists of 10000 samples generated from the illustrative model specified in Example 1. For Figures 5a and 5b, we used 100 samples from this dataset.

Since, under the iid assumption,  $\frac{\mathbf{y}^\top \mathbf{y}}{n}$ ,  $\frac{\mathbf{X}^\top \mathbf{y}}{n}$ , and  $\frac{\mathbf{X}^\top \mathbf{X}}{n}$  converge element-wise as  $n$  increases and  $T_{\mathbf{t}}$  is independent of  $n$ , we would like to choose  $\delta$  such that  $L_{\mathbf{t}}^{-1}$  also converges as  $n$  increases. To achieve this, first observe that

$$L_{\mathbf{t}} = T_{\mathbf{t}} \left( \frac{\mathbf{X}^\top \mathbf{X}}{n} \right) T_{\mathbf{t}} + \frac{\delta}{n} (I - T_{\mathbf{t}}^2).$$

It is then evident that the choice  $\delta = cn$  for a fixed constant  $c$ , independent of  $n$ , makes  $L_{\mathbf{t}}$  converging as  $n$  increases, and specifically, the choice  $c = 1$  justifies the behavior observed in Figure 5.

## 5.2 Controlling the Sparsity through $\lambda$

Intuitively, it is clear that larger the value of  $\lambda$  the sparser the solution offered by COMBSS, when all other parameters are fixed. We strengthen this understanding, first visually and then also mathematically.

Visually, from Figure 2, we can understand that by selecting a suitable positive  $\lambda$  we can make COMBSS converge towards a sparse solution  $s^*$ , which is in fact the optimal solution. Figure 6 shows that, for the illustrative model in Example 1, if we take the value of  $\lambda$  to be very high, we can push the algorithm to converge to a much more sparse solution, in this case, that point being  $(0,0)^\top$ .

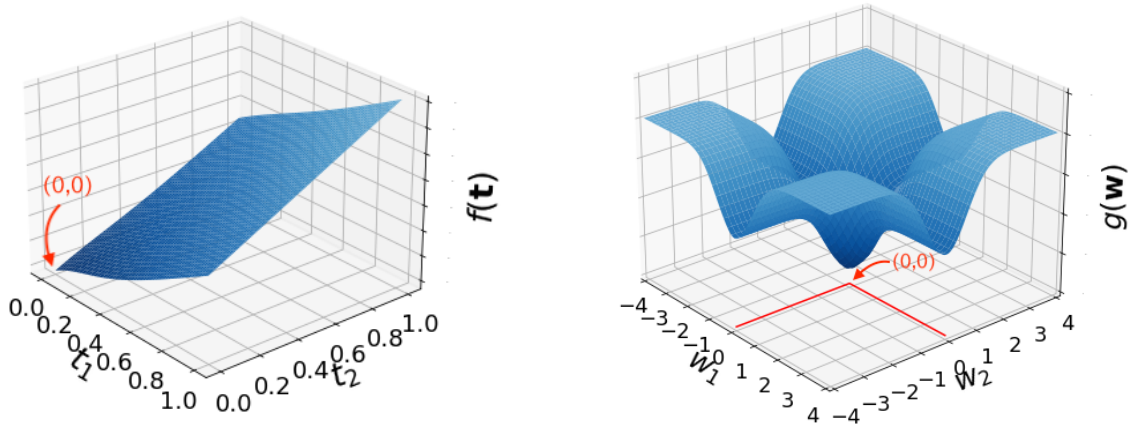


Figure 6: Illustration of effects of large  $\lambda$  on the curvature of  $f_\lambda(\mathbf{t})$  and  $g_\lambda(\mathbf{w})$ . Here, the data is generated from the model considered in Example 1 and  $\lambda = 100$ .

Mathematically, from Theorem 4,

$$\nabla f_\lambda(\mathbf{t}) = \zeta_{\mathbf{t}} + \lambda \mathbf{1}, \quad \mathbf{t} \in (0, 1)^p,$$

and

$$\nabla g_\lambda(\mathbf{w}) = (\zeta_{\mathbf{t}} + \lambda \mathbf{1}) \odot (2\mathbf{w} \odot \exp(-\mathbf{w} \odot \mathbf{w})), \quad \mathbf{w} \in \mathbb{R}^p,$$

where  $\zeta_{\mathbf{t}}$ , given by (15), is independent of  $\lambda$ . We note the following property of  $\zeta_{\mathbf{t}}$ .

**Proposition 1.** For any  $j = 1, \dots, p$ , if we fix  $t_i$  for  $i \neq j$ ,

$$\lim_{t_j \downarrow 0} \zeta_{\mathbf{t}}(j) = 0.$$

A proof of Proposition 1 is given in Appendix A. This result implies that for any  $j = 1, \dots, p$ ,

$$\lim_{t_j \downarrow 0} \frac{\partial f_\lambda(\mathbf{t})}{\partial t_j} = \lambda,$$

where  $\lim_{t_j \downarrow 0}$  denotes the existence of the limit for any sequence of  $t$  that is converging to 0 from right. Since  $\zeta_{\mathbf{t}}$  is independent of  $\lambda$ , the above limit implies that there is a window  $(0, a_j)$  such

that the slope  $\frac{\partial f_\lambda(\mathbf{t})}{\partial t_j} > 0$  for  $t_j \in (0, a_j)$  and also the window size increases (i.e.,  $a_j$  increases) as  $\lambda$  increases. As a result, for the function  $g_\lambda(\mathbf{w})$ , there exists a constant  $a'_j$  such that

$$\frac{\partial g_\lambda(\mathbf{w})}{\partial w_j} \begin{cases} < 0, & \text{for } a'_j < t_j < 0 \\ > 0, & \text{for } 0 < t_j < a'_j. \end{cases}$$

In other words, for positive  $\lambda$ , there is a ‘valley’ on the surface of  $g_\lambda(\mathbf{w})$  along the line  $w_j = 0$  and the valley becomes deeper and wider as  $\lambda$  increases. In summary, the larger the values of  $\lambda$  the more  $w_j$ ’s (or, equivalently  $t_j$ ) are pushed towards 0 by the algorithm and then a sparse model is selected (i.e, small number  $k$  of variables chosen). At the extreme a value  $\lambda_{\max} = \|y\|_2^2/n$  will force all the  $t_j$  to be equal to 0 and the null model will be selected.

In practice, this tuning parameter  $\lambda$  is generally calibrated by defining a grid of  $\lambda$  values and then exploits  $K$ -fold cross-validation procedures (e.g., [26]) or model selection criterion (e.g., [1, 24, 5]).

## 6 Efficient Implementation of COMBSS

In this section, we focus on efficient implementation of COMBSS using the *conjugate gradient* method, the *Woodbury matrix identity*, and the *Banachiewicz Inversion Formula*.

Almost all the computational cost (or, the running time) of COMBSS is dictated by the gradient descent method used at Step 1 of Algorithm 1, which in-turn depends on how fast the gradient  $\nabla g_\lambda(\mathbf{w})$  is computed in each iteration of the gradient descent algorithm. For instance, in the basic gradient descent algorithm, the point  $\mathbf{w}^{(l)}$  at the  $l$ -th iteration is computed by

$$\mathbf{w}^{(l)} = \mathbf{w}^{(l-1)} - \alpha \nabla g_\lambda(\mathbf{w}^{(l-1)}),$$

using the point  $\mathbf{w}^{(l-1)}$  from the previous iteration; see Appendix B for more details on gradient descent methods.

First, in Section 6.1, we show how to estimate the gradients  $\nabla g_\lambda(\mathbf{w})$  using the conjugate gradient, an efficient method for solving linear equations. Then, in Section 6.2, we specifically focus on the high-dimensional case (i.e.,  $n < p$ ) and propose an approach to reduce the dimension of the linear equation problem solved by the conjugate gradient. In Section 6.3, we propose another dimension reduction approach that ignores the columns of the design matrix  $X$  correspond to  $w_j = 0$  for computing the gradients. Finally, in Section 6.4, we put all these ideas together to make COMBSS fast.

### 6.1 Estimation of Gradients using Conjugate Gradient

Recall the expression of  $L_t$  from (6):

$$L_t = \frac{1}{n} \left[ X_t^\top X_t + \delta (I - T_t^2) \right].$$

We have noticed earlier from Theorem 4 that the exact computation of  $\nabla g_\lambda(\mathbf{w})$  requires computing  $L_t^{-1}$ , which can be expensive. However, fortunately, all we really need for computing  $\nabla g_\lambda(\mathbf{w})$  is

evaluating matrix-vector products of the form  $L_t^{-1}\mathbf{u}$ , which is the unique solution of the linear equation  $L_t\mathbf{z} = \mathbf{u}$  for all  $\mathbf{t} \in [0, 1]^p$  (refer to Theorem 1 for invertibility of  $L_t$  for all  $\mathbf{t} \in [0, 1]^p$ ). Furthermore, the performance of the gradient descent method does not change significantly as long as a good approximation of the gradient  $\nabla g_\lambda(\mathbf{w})$  is provided. As a result, it is optimal to seek efficient techniques for solving  $L_t\mathbf{z} = \mathbf{u}$ .

Solving linear equations efficiently is one of the important and well studied problems in the field of linear algebra, and there are several elegant approaches in the literature to address this problem. The Krylov subspace methods, a family of iterative methods for solving linear equations, are most popular in the literature for solving  $A\mathbf{z} = \mathbf{u}$  efficiently just by using the matrix-vector product  $A\mathbf{u}$  (or,  $A^\top\mathbf{u}$ ), see for instance, [11]. Among these methods, the conjugate gradient method is well-known to work efficiently for the problems where  $A$  is symmetric positive-definite and can achieve a close approximation to  $A^{-1}\mathbf{u}$  within  $O(p^2)$  time. Since,  $L_t$  is a symmetric positive-definite matrix, we can simply use any standard software package for the conjugate gradient method in the implementation of COMBSS.

## 6.2 Low-dimension vs High-dimension

As noticed in the previous subsection, the running time of the conjugate gradient method for solving  $A\mathbf{z} = \mathbf{u}$  depends on the dimension of  $A$ . In particular, since  $L_t$  is of dimension  $p \times p$ , the conjugate gradient method can return an approximation of  $L_t^{-1}\mathbf{u}$  within  $O(p^2)$  time by fixing the maximum number of iterations taken by the conjugate gradient method. This is true for both low-dimensional models (where  $p < n$ ) and high-dimensional models (where  $n < p$ ).

Below, we specifically focus on high-dimensional models and transform the problem of solving the  $p$ -dimensional linear equation  $L_t\mathbf{z} = \mathbf{u}$  to the problem of solving an  $n$ -dimensional linear equation problem. This approach is based on a well-known result in linear algebra called the Woodbury matrix identity. Since we are calling the gradient descent method for solving a  $n$ -dimensional problem (instead of  $p$ -dimensional), we can achieve a much lower overall computational complexity for the high-dimensional models.

The following result is a consequence of the Woodbury matrix identity; refer to Appendix A for a proof.

**Theorem 5.** For  $\mathbf{t} \in [0, 1]^p$ , let  $S_t$  be a  $p$ -dimensional diagonal matrix with the  $j$ -th diagonal element being  $n/\delta(1-t_j^2)$  and

$$\tilde{L}_t := I + \frac{1}{n}X_t S_t X_t^\top.$$

Then,

$$L_t^{-1}\mathbf{u} = (S_t\mathbf{u}) - \frac{1}{n}S_t X_t^\top \tilde{L}_t^{-1} (X_t S_t \mathbf{u}).$$

The above expression suggests that instead of solving the  $p$ -dimensional problem  $L_t\mathbf{z} = \mathbf{u}$  directly, we can first solve the  $n$ -dimensional problem  $\tilde{L}_t\mathbf{z} = (X_t S_t \mathbf{u})$  and substitute the result in the above expression to get the value of  $L_t^{-1}\mathbf{u}$ . As a consequence, for high-dimensional models, we can achieve smaller running times by this indirect approach for computing the gradients in the execution of gradient descent algorithm.

### 6.3 A Dimension Reduction Approach

During the execution of the gradient descent algorithm, Step 1 of Algorithm 1, some of the  $w_j$ 's (and hence  $t_j$ 's) can reach zero. Particularly, for the basic gradient descent method, once  $w_j$  reaches zero it continues to be zero until the algorithm terminates. This is because, as mentioned earlier, the update of  $\mathbf{w}$  in the  $l$ -th iteration of the basic gradient descent depends only on the gradient  $g_\lambda(\mathbf{w}^{(l)})$ , whose  $j$ -th element

$$\frac{\partial g_\lambda(\mathbf{w}^{(l)})}{\partial w_j} = 0 \quad \text{if } w_j^{(l)} = 0. \quad (16)$$

Based on the fact that (16) holds, we ask: Can we just focus only on the terms  $\frac{\partial g_\lambda(\mathbf{w})}{\partial w_j}$  associated with  $w_j \neq 0$  in order to reduce the computation cost of computing the gradient  $\nabla g_\lambda(\mathbf{w})$ ? The answer is yes, and below we provide an approach for achieving this.

To simplify the notation, let  $\mathcal{P} = \{1, \dots, p\}$  and for any  $\mathbf{t} = (t_1, \dots, t_p)^\top \in [0, 1]^p$ , let  $\mathcal{Z}_\mathbf{t}$  be the set of indices of the zero elements of  $\mathbf{t}$ , that is,

$$\mathcal{Z}_\mathbf{t} = \{j : t_j = 0, j \in \mathcal{P}\}. \quad (17)$$

For a vector  $\mathbf{u} \in \mathbb{R}^p$ , we write  $(\mathbf{u})_+$  (respectively,  $(\mathbf{u})_0$ ) to denote the vector of dimension  $p - |\mathcal{Z}_\mathbf{t}|$  (respectively,  $|\mathcal{Z}_\mathbf{t}|$ ) constructed from  $\mathbf{u}$  by removing all its elements with the indices in  $\mathcal{Z}_\mathbf{t}$  (respectively, in  $\mathcal{P} \setminus \mathcal{Z}_\mathbf{t}$ ). Similarly, for a matrix  $A$  of dimension  $p \times p$ , we write  $(A)_+$  (respectively,  $(A)_0$ ) to denote the new matrix constructed from  $A$  by removing its rows and columns with the indices in  $\mathcal{Z}_\mathbf{t}$  (respectively, in  $\mathcal{P} \setminus \mathcal{Z}_\mathbf{t}$ ). Then we have the following result.

**Theorem 6.** *Suppose  $\mathbf{t} \in [0, 1]^p$ . Then,*

$$(L_\mathbf{t})_+ = \frac{1}{n} \left[ (T_\mathbf{t})_+ \left( X^\top X \right)_+ (T_\mathbf{t})_+ + \delta (I - (T_\mathbf{t})_+) \right].$$

Furthermore, we have

- (i)  $(L_\mathbf{t}^{-1})_0 = \frac{n}{\delta} I$  and  $(L_\mathbf{t}^{-1})_+ = ((L_\mathbf{t})_+)^{-1}$ ;
- (ii)  $(\tilde{\beta}_\mathbf{t})_0 = \mathbf{0}$  and  $(\tilde{\beta}_\mathbf{t})_+ = ((L_\mathbf{t})_+)^{-1} \left( (\mathbf{t})_+ \odot \left( \frac{X^\top \mathbf{y}}{n} \right)_+ \right)$ ;
- (iii)  $(\mathbf{c}_\mathbf{t})_0 = \mathbf{0}$  and  $(\mathbf{c}_\mathbf{t})_+ = ((L_\mathbf{t})_+)^{-1} ((\mathbf{t})_+ \odot (\mathbf{a}_\mathbf{t})_+)$ .

A proof of Theorem 6 is given in Appendix A. Theorem 6 (i) is based on the Banachiewicz Inversion Formula (Lemma 1 in Appendix A). It shows that for every  $j \in \mathcal{Z}_\mathbf{t}$ , all the off-diagonal elements of the  $j$ -th row and the  $j$ -th column of  $L_\mathbf{t}^{-1}$  are zero while its  $j$ -th diagonal element is  $n/\delta$ , and all other elements of  $L_\mathbf{t}^{-1}$  (which constitute the sub-matrix  $(L_\mathbf{t}^{-1})_+$ ) depend only on  $(L_\mathbf{t})_+$ , which can be computed using only the columns of the design matrix  $X$  with indices in  $\mathcal{P} \setminus \mathcal{Z}_\mathbf{t}$ . As a consequence, (ii) and (iii) imply that computing  $\tilde{\beta}_\mathbf{t}$  and  $\mathbf{c}_\mathbf{t}$  is equal to solving  $p_+$ -dimensional linear equations of the form  $(L_\mathbf{t}^{-1})_+ \mathbf{z} = \mathbf{v}$ , where

$$p_+ = p - |\mathcal{Z}_\mathbf{t}|.$$

Since  $p_+ \leq p$ , solving such a  $p_+$ -dimensional linear equation using the conjugate gradient can be faster than solving the original  $p$ -dimensional linear equation of the form  $L_{\mathbf{t}}\mathbf{z} = \mathbf{u}$ .

In summary, for a vector  $\mathbf{t} \in [0, 1]^p$  with some elements being 0, the values of  $f_\lambda(\mathbf{t})$  and  $\nabla f_\lambda(\mathbf{t})$  do not depend on the columns  $j$  of  $X$  where  $t_j = 0$ . Therefore, we can reduce the computational complexity by removing the all columns  $j$  of the design matrix  $X$  where  $t_j = 0$ .

## 6.4 Making COMBSS Fast

In Section 6.3, we noted that when some elements  $t_j$  of  $\mathbf{t}$  are zero, it is faster to compute the objective functions ( $f_\lambda(\mathbf{t})$  and  $g_\lambda(\mathbf{t})$ ) and their gradients ( $\nabla f_\lambda(\mathbf{t})$  and  $\nabla g_\lambda(\mathbf{t})$ ) by ignoring the columns  $j$  of the design matrix  $X$ . This is because the effective dimension of the design matrix is  $n \times p_+$ .

In Section 5.2, using Proposition 1, we have observed that for any  $\lambda > 0$  there is a ‘valley’ on the surface of  $g_\lambda(\mathbf{w})$  along  $w_j = 0$  for all  $j = 1, \dots, p$ . As a consequence, we have also observed that for any  $j$ , when  $w_j$  (or, equivalently,  $t_j$ ) is sufficiently small during the execution of the gradient descent method, it will eventually become 0, as it can not escape the valley. For instance, consider the example illustrated in Figure 7. We observe that many of the  $t_j$ ’s reached values close to zero within the first 60 iterations, and by the 80-th iteration, except one, the values of all  $t_j$ ’s correspond to zero  $\beta_j$ ’s in the true model are zero or insignificantly small. This sparsity in  $\mathbf{t}$  is much more pronounced, when moving to 100 iterations and then to the final iteration.

As a consequence, in the implementation of COMBSS, to reduce the computational cost of estimating the gradients during the execution of the gradient descent method, it is wise to map  $w_j$  (and  $t_j$ ) to 0 when  $w_j$  is almost zero. We incorporate this truncation idea as follows. We first fix a small constant  $\eta$ , say  $\eta = 0.001$ . As we run the gradient descent algorithm, when  $t_j$  becomes smaller than  $\eta$  for some  $j \in \mathcal{P}$ , we take  $t_j$  and  $w_j$  to be zero and we stop updating them any further (that is,  $t_j$  and  $w_j$  will continue to be zero until the gradient descent algorithm terminates). In each iteration of the gradient descent algorithm, the design matrix is updated by removing all the columns corresponding to zero  $t_j$ ’s. If the algorithm starts at  $\mathbf{w}$  with all non-zero elements, the effective dimension  $p_+$ , which denotes the number of columns in the updated design matrix, monotonically decreases starting from  $p$ . In an iteration, if  $p_+ > n$ , we can use Theorem 5 to reduce the complexity of computing the gradients. On the other hand, when  $p_+$  falls below  $n$ , we directly use conjugate gradient for computing the gradients without invoking Theorem 5.

The following list summarizes the key steps we take to make COMBSS fast:

1. We use the well-known Adam optimizer to minimize the objective function  $g_\lambda$  for any given  $\lambda$ ; refer to Figure 3 to see that the Adam optimizer converges faster than the basic gradient descent.
2. In every iteration of the gradient descent, we truncate all the  $t_j$  (and hence the corresponding  $w_j$ ) to zero if they are smaller than the pre-selected truncation parameter  $\eta$ . That is, for any  $j \in \mathcal{P}$ , we assign 0 to both  $t_j$  and  $w_j$  if  $t_j < \eta$ .
3. In any iteration of the gradient descent, we invoke the Woodbury matrix identity via Theorem 5 in computing  $L_{\mathbf{t}}^{-1}\mathbf{u}$  if and only if  $p_+ > n$ .

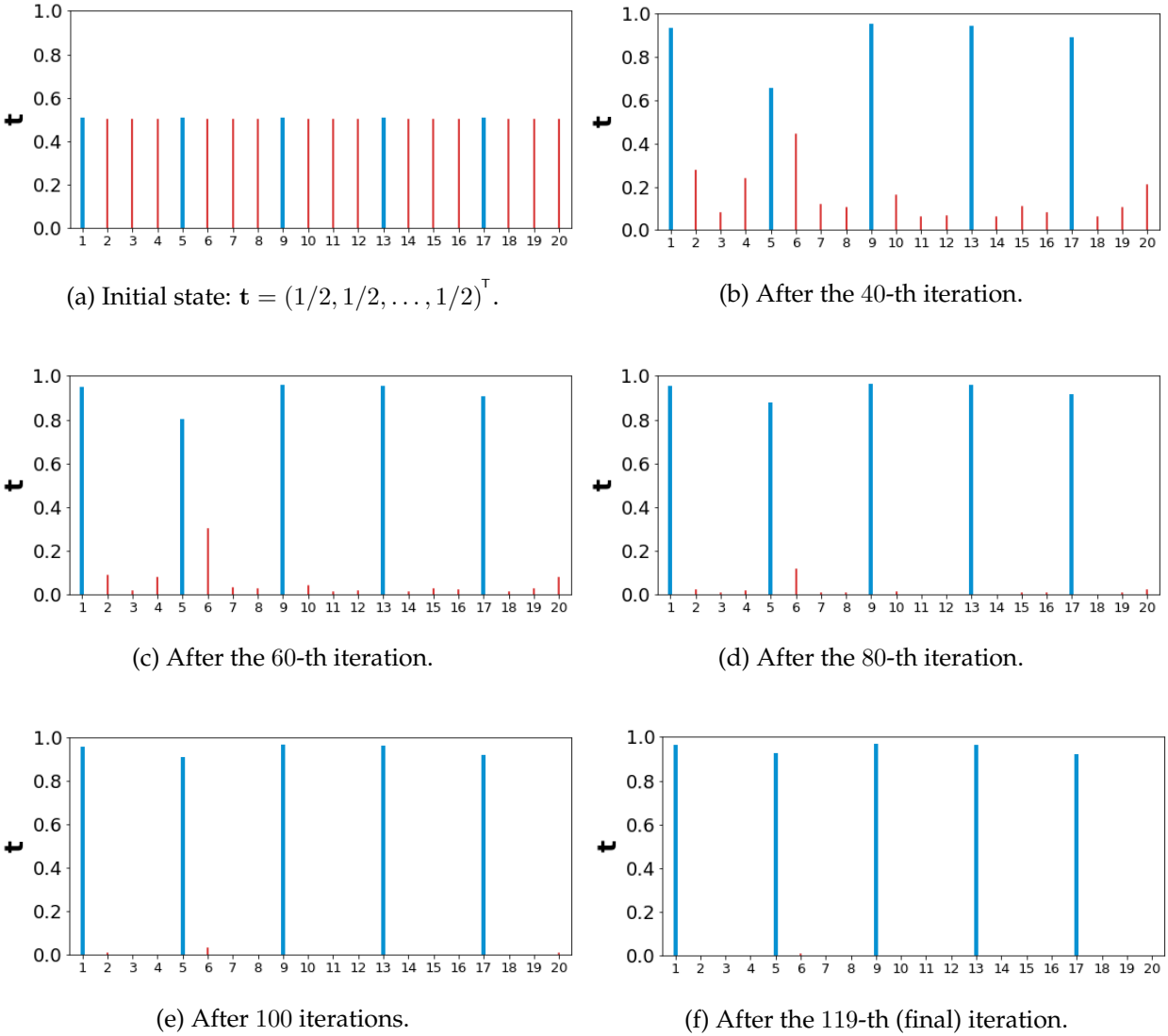


Figure 7: Illustration of convergence of  $\mathbf{t}$  during the execution of the basic gradient descent for an example dataset generated using Beta-type 1 with  $k_0 = 5$ ,  $p = 20$ ,  $n = 100$ ,  $\rho = 0.5$ , and  $\text{SNR} = 3$ ; see Section 7 for more details on data generation. Here, we have taken  $\lambda = 0.2$  and  $\delta = n$ . The set of indices of the (thick) blue bars correspond to the non-zero elements in the true coefficient vector  $\beta$ , and (thin) red bars correspond to the zero elements in  $\beta$ . The height of the  $j$ -th bar denotes the value of  $t_j$ .

4. Whenever we need to compute an expression of the form  $A^{-1}\mathbf{u}$ , we use the conjugate gradient method to solve the linear equation  $Az = \mathbf{u}$  to obtain an approximation of  $A^{-1}\mathbf{u}$ .

Figure 8 illustrates that COMBSS is substantially much faster when the above mentioned improvement ideas are incorporated in its implementation.

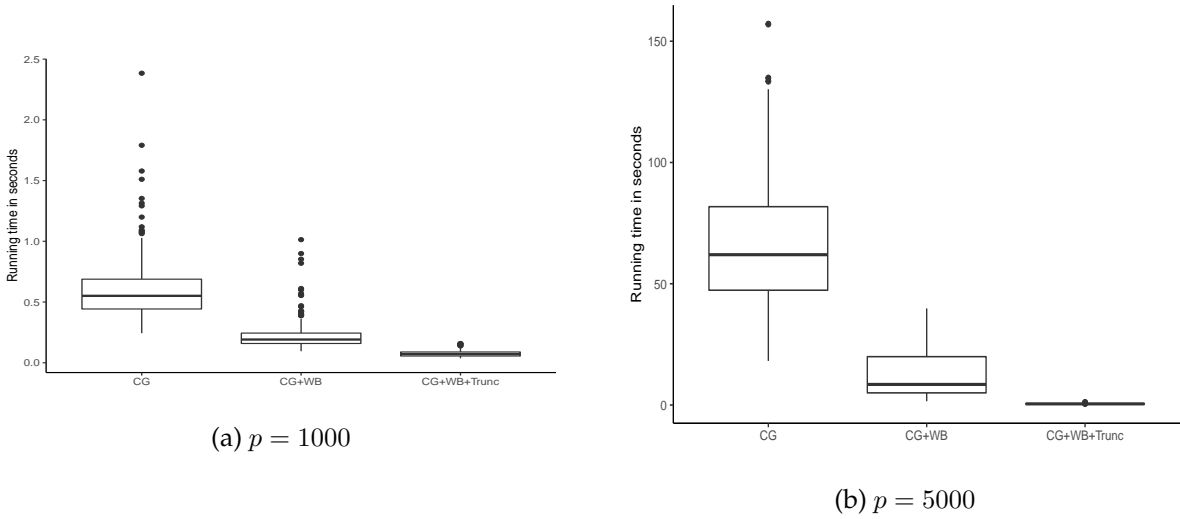


Figure 8: Running time of execution of COMBSS (until convergence with respected to max-norm) for  $\lambda = 0.1$  for dataset generated using Beta-type 1 with  $k_0 = 5$ ,  $n = 100$ ,  $p = 1000$ ,  $\rho = 0.8$ , and  $\text{SNR} = 5$  (same as for Figures 3 and 4). The boxplot are based on 300 replications. Here we compare running times for COMBSS using only conjugate gradient (CG), conjugate gradient with Woodbury matrix identity (CG + WB), and conjugate gradient with both Woodbury matrix identity and truncation improvement (CG +WB + Trunc). For the truncation,  $\eta = 0.001$ .

## 7 Simulation Experiments

In this section, through empirical research, we assess the efficiency and correctness of our proposed method, COMBSS, and compare it with two main existing methods, Forward Selection (FS) and MIO, for solving the best subset selection problem. We also add to the comparison the popular Lasso model, which is not a best subset method.

Even if our method was motivated by the challenge of features extraction for high-dimensional data sets, it is important and instructive to also investigate the behaviour of our approach in a low dimensional setting compared to traditional ones, so we consider both, traditional and high-dimensional settings.

### 7.1 Simulation Setting

The data is generated from the linear model:

$$\mathbf{y} = X\boldsymbol{\beta} + \boldsymbol{\epsilon}, \quad \text{where } \boldsymbol{\epsilon} \sim N_n(0, \sigma^2 \mathbb{I}_n), \quad (18)$$

where each row of the predictor matrix  $X$  is generated from a multivariate normal distribution with zero mean and covariance matrix  $\Sigma$  with diagonal elements  $\Sigma_{j,j} = 1$  and off-diagonal elements  $\Sigma_{i,j} = \rho^{|i-j|}$ ,  $i \neq j$ , for some correlation parameter  $\rho \in (-1, 1)$ . In order to investigate a challenging situation, we use  $\rho = 0.8$  to mimic strong correlation between predictors. For each

simulation, we fix the signal-to-noise ratio (SNR) and compute the variance  $\sigma^2$  of the noise  $\epsilon$  using

$$\sigma^2 = \frac{\boldsymbol{\beta}^\top \boldsymbol{\Sigma} \boldsymbol{\beta}}{\text{SNR}}.$$

We consider the following two simulation settings (also used in [4]):

- **Beta-type 1:**  $k_0 = 10$  components of  $\boldsymbol{\beta}$  are equal to 1 at equally spaced indices between 1 and  $p$ , and all other components of  $\boldsymbol{\beta}$  are 0.
- **Beta-type 2:** The first  $k_0 = 10$  components of  $\boldsymbol{\beta}$  are equal to 1 and all other components of  $\boldsymbol{\beta}$  are equal to 0.

The Beta-type 1 situation will provide low correlation between active predictors while Beta-type 2 assumes strong correlation between the active predictors. For both these types, we investigate the performance of our method in low- and high-dimensional settings. For the low-dimensional setting, we take  $n = 100$  and  $p = 20$  for  $\text{SNR} \in \{0.5, 1, 2, \dots, 8\}$ , while for the high-dimensional setting,  $n = 100$  and  $p = 1000$  for  $\text{SNR} \in \{2, 3, \dots, 8\}$ .

The comparison between the methods are given in terms of prediction error and variable selection accuracy performances. The prediction error (PE) performance of a method is defined as

$$\text{PE} = \left\| X\hat{\boldsymbol{\beta}} - X\boldsymbol{\beta} \right\|_2^2 / \|X\boldsymbol{\beta}\|_2^2,$$

where  $\hat{\boldsymbol{\beta}}$  is the estimated coefficient obtained by the method. The variable selection accuracy performances used are: sensibility (true positive rate), specificity (true negative rate), accuracy,  $F_1$  score, and the Mathew's correlation coefficient (MCC) [6].

## 7.2 Model Tunning

In the low-dimensional setting, FS and MIO were tuned over  $k = 0, \dots, 20$ . For the high dimensional setting, FS was tuned over  $k = 0, \dots, 50$ , while MIO was tuned over  $k = 0, \dots, 30$  only due to time computational constraints. We re-observed that MIO based on the Gurobi optimizer is quite time consuming for high dimensional cases (see [14]). In this simulation we ran MIO through the R package `bestsubset` offered in [13] and we fixed the default budget to 1 minute 40 seconds (per problem per  $k$ ).

In low and high dimensional settings, the Lasso was tuned for 50 values of  $\lambda$  ranging from  $\lambda_{\max} = \|X^T \mathbf{y}\|_\infty$  to a small fraction of  $\lambda_{\max}$  on a log scale, as per the default in `bestsubset` package. In both the low- and high-dimensional settings, COMBSS was also tuned using 50 values of  $\lambda$  ranging from  $\lambda_{\max} = \|\mathbf{y}\|_2^2 / n$  to a small fraction of  $\lambda_{\max}$ . To be precise the 50 values of  $\lambda$  are defined by  $\lambda_l = \lambda_{\max} \times 0.8^{(l-1)}$  with  $l = 1, \dots, 50$ . Further, we have set  $\eta = 0.001$ ,  $\tau = 0.5$ , and  $\delta = n$  (involved in  $L_t$ ). For all the simulations, we use Adam optimizer with  $\alpha = 0.1$ ,  $\xi_1 = 0.9$ , and  $\xi_2 = 0.999$  (see Appendix B.2).

For each subset size  $k$  for FS and MIO and each tuning parameter  $\lambda$  for Lasso and COMBSS, we evaluate the mean square error (MSE) using a validation set of 500 samples from the true model defined in (18). Then, for all the four methods, the best model is the one with the lowest MSE.

### 7.3 Simulation Results

Figure 9 presents the results in the low dimensional setting for both Beta-type 1 and Beta-type 2. The panels in this figure display the average of MCC, accuracy and prediction error over 500 replications for the four procedures, and vertical bars denote one standard error. The other metrics ( $F_1$ , sensitivity and specificity) are presented in Figure 11 in Appendix C.

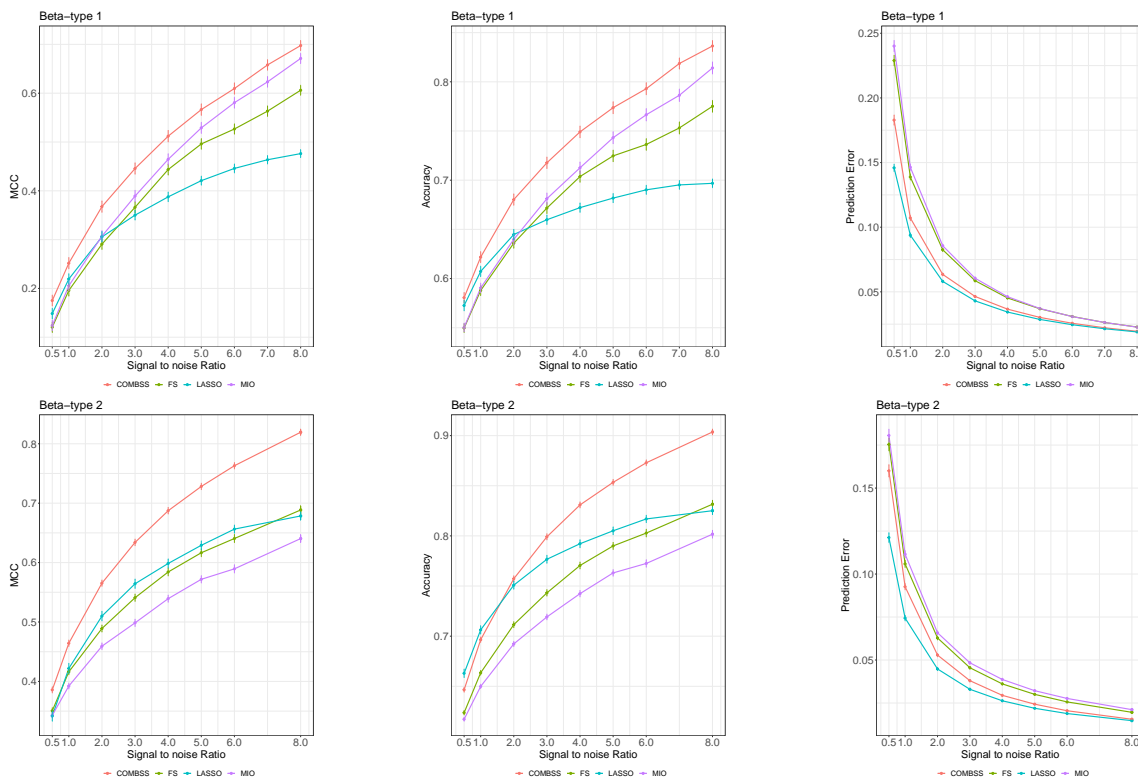


Figure 9: Performance results in terms of MCC, accuracy and prediction error, for the low-dimensional cases:  $n = 100$ ,  $p = 20$ ,  $\rho = 0.8$ , and true active predictor is 10 with Beta-type 1 (top plots) and Beta-type 2 (bottom plots).

Overall, COMBSS outperforms the FS and MIO procedures in terms of MCC, accuracy, and prediction error. It also outperforms the Lasso in terms of MCC and accuracy even for Beta-type 2 (high correlation of the true active signal) and for small SNR, both the approaches give similar results. We can see that FS and MIO have similar pattern for Beta-type 1 while FS seems to be preferable for Beta-type 2, where there the true set of variables are highly correlated. Note that the Lasso presents lower prediction error in general as it tends to provide dense model compared to other methods. As a result, the Lasso suffers with low specificity which is clearly exhibited in Figure 11 in Appendix C.

Figure 10 presents the results in the high-dimensional setting for both Beta-type 1 and Beta-type 2. The panels in this figure display average MCC and prediction error over 10 replications for all the four methods, and vertical bars denote one standard error. The other metrics ( $F_1$ , sensitivity, and specificity) are presented in Figure 12 in Appendix C. We do not present accuracy for the high-dimensional setting, because even a procedure which always selects the null model will get

an accuracy of  $990/1000 = 0.99$ ). We restrict this simulation to 10 replications due to the time constraint of running MIO in this setting. Even if the other approaches have been ran other 500 replications easily, we present here only the results on the same 10 repetitions.

For the Beta-type 1 scenario, the three best subset selection methods (FS, MIO and COMBS) give similar results and outperform the Lasso in terms of MCC. In this situation, the Lasso obtains lower prediction error for lower SNR but still suffers from selecting dense models and thus gets small specificity (see 12 in Appendix C). Overall, COMBSS outperforms the other procedures in the Beta-type 2 scenario.

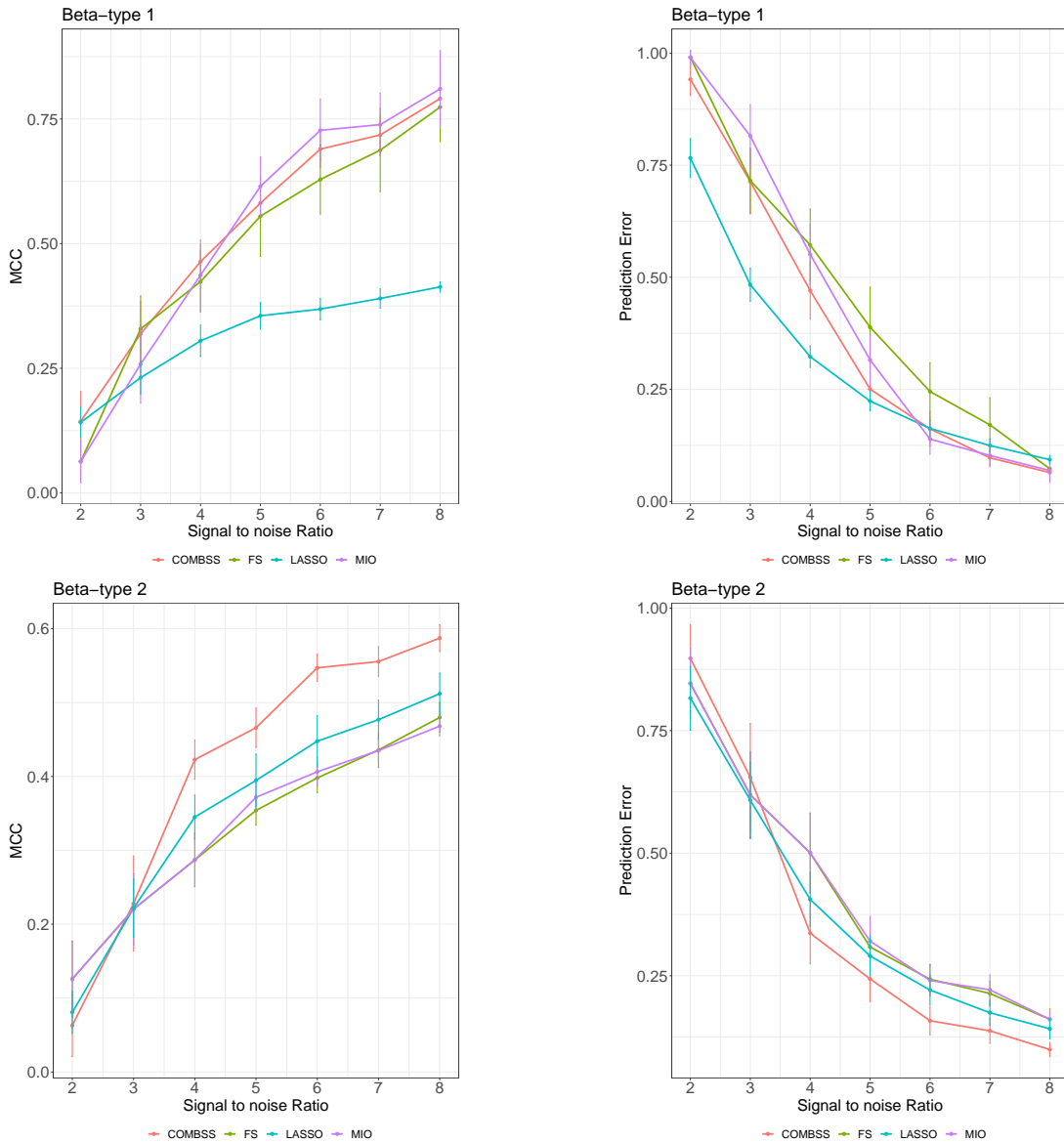


Figure 10: Performance results in terms of MCC and prediction error, for the high-dimensional cases:  $n = 100$ ,  $p = 1000$ ,  $\rho = 0.8$ , and true active predictor is 10 with Beta-type 1 (top plots) and Beta-type 2 (bottom plots).

## 8 Discussion

In this paper, we have introduced COMBSS, a novel continuous optimization method that solves the best subset selection problem in linear regression, particularly when the number of features  $p$  is very large. Key goal of COMBSS is to extend the highly complex discrete constrained best subset selection problem to an unconstrained continuous optimization problem. In particular, COMBSS involves extending the objective function of the best subset selection, which is defined at the corners of the hypercube  $[0, 1]^p$ , to a differentiable function defined on the whole hypercube. For this extended function, starting from an interior point, a gradient descent method converges to a corner where the minimum for the best subset selection problem is achieved.

The major technological innovations were made in the coding of COMBSS and we have made Python and R codes available at <https://github.com/saratmoka/COMBSS-Python-VIGNETTE> and <https://github.com/benoit-liquet/COMBSS-R-VIGNETTE>, respectively. In this article, we have specifically highlighted some of the steps that make COMBSS computationally fast, including using conjugate gradient and other linear algebra techniques. In our implementation of COMBSS, the primary operations involved are matrix-vector product, vector-vector element-wise product, and scalar-vector product (noting that the primary operation for executing a conjugate gradient method for solving a linear equation  $Az = \mathbf{u}$  is the matrix-vector product  $A\mathbf{u}$ ). All these operations are known to execute faster on GPU based computers using parallel programming. Such parallel programming based implementation of COMBSS could substantially increase its speed.

In the paper, we have conducted several simulation experiments in both low-dimensional and high-dimensional setups to illustrate the good performance of COMBSS in comparison to the existing popular methods: Forward Stepwise, Lasso, and Mixed Integer Optimization. These promising empirical results highlight the potential of COMBSS for feature extractions. We leave extensive performance comparisons with Lasso variants such as relaxed Lasso [20] and best subset selection based on coordinate descent and local combinatorial optimization [15] to future work.

We highlight that the primary focus of this paper was to introduce the novel COMBSS approach to exhaustive feature selection and illustrate its performance. In ongoing work, we are incorporating additional tricks and functionality to make COMBSS even faster and more user-friendly. We expect, similarly to the significant body of work that focuses on the Lasso and on MIO, respectively, that there are many avenues that can be explored and investigated for building on the presented COMBSS framework. Particularly, to tackle the best subset selection when problems are of ultra high dimensional.

The following is a partial list of considerations and future research, that goes beyond the scope of this article.

- Despite using the same grid of  $\lambda$  values for COMBSS in all our simulations, it is competitive with all the existing methods considered in this paper. Future work on more efficient selection of the grid may further enhance the performance of COMBSS. As with all feature selection methods where the tuning of parameters is part of the challenge, future research is needed to appropriately investigate to what extent insights into the tuning of the Lasso and other regularisation methods translates to the tuning of COMBSS.

- Although, in this paper, COMBSS achieves sparsity via  $\sum_{j=1}^p t_j$ , which turns out to be the  $\mathcal{L}_1$ -norm of  $\mathbf{t}$  because  $\|\mathbf{t}\|_1 = \sum_{j=1}^p t_j$  for  $\mathbf{t} \in [0, 1]^p$ . However, regularising with the  $\mathcal{L}_1$ -norm is not crucial and in fact sparsity in the solution of COMBSS can be achieved using other norms; for example we could replace  $\sum_{j=1}^p t_j$  with  $\|\mathbf{t}\|_r^r = \sum_{j=1}^p t_j^r$  for  $r \geq 1$ . Future work could focus on the selection of an optimal metric for the penalty term in COMBSS.
- In this paper, we explore first-order continuous optimization methods for executing COMBSS. The learning rate parameter  $\alpha$  of these methods can influence their performance. Since, it is possible to compute the second-order derivatives of the objective functions  $f_\lambda$  and  $g_\lambda$ , future work can improve the performance of COMBSS by exploiting second-order methods to avoid the calibration of the learning rate.
- Recall that the purpose of the mapping  $t_j(w_j) = 1 - \exp(-w_j^2)$  in is to convert the boxed constrained optimization problem (10) to the unconstrained optimization problem (14). We note that any strictly increasing function on  $\mathbb{R}_+$  that starts with 0 at 0 and goes to 1 as  $w_j \rightarrow \infty$  will also convert the boxed constrained optimization problem to the unconstrained optimization problem. For instance, we could consider  $t_j(w_j) = \tanh(w_j^2)$ . Finding an optimal such function could be a part of future work.

In conclusion, to the best of our knowledge, COMBSS is the first method that exploits unconstrained continuous optimization to solve best subset selection in linear regression. As highlighted in this discussion and throughout the article, COMBSS potentially opens a new avenue of research in high-dimensional feature selection, going well beyond the linear regression model.

## A Proofs

*Proof of Theorem 1.* Since both  $X_{\mathbf{t}}^\top X_{\mathbf{t}}$  and  $T_{\mathbf{t}}$  are symmetric, the symmetry of  $L_{\mathbf{t}}$  is obvious. We now show that  $L_{\mathbf{t}}$  is positive-definite for  $\mathbf{t} \in [0, 1]^p$  by establishing

$$\mathbf{u}^\top L_{\mathbf{t}} \mathbf{u} > 0, \quad \text{for all } \mathbf{u} \in \mathbb{R}^p \setminus \{\mathbf{0}\}. \quad (19)$$

Trivially,  $X_{\mathbf{t}}^\top X_{\mathbf{t}}$  is a positive semi-definite matrix, because

$$\mathbf{u}^\top X_{\mathbf{t}}^\top X_{\mathbf{t}} \mathbf{u} = \|X_{\mathbf{t}} \mathbf{u}\|_2^2 \geq 0.$$

In addition, for all  $\mathbf{t} \in [0, 1]^p$ ,  $\delta (I - T_{\mathbf{t}}^2)$  is a positive definite matrix due to the fact that  $\delta > 0$  and

$$\begin{aligned} \mathbf{u}^\top (I - T_{\mathbf{t}}^2) \mathbf{u} &= \|\mathbf{u}\|_2^2 - \|T_{\mathbf{t}} \mathbf{u}\|_2^2 \\ &= \sum_{j=1}^p u_{j+1}^2 (1 - t_j^2), \end{aligned} \quad (20)$$

which is strictly positive if  $\mathbf{t} \in [0, 1]^p$  and  $\mathbf{u} \in \mathbb{R}^p \setminus \{\mathbf{0}\}$ .

Since positive definite matrices are invertible, we have  $L_{\mathbf{t}}^+ = L_{\mathbf{t}}^{-1}$ , and thus,  $\tilde{\beta}_{\mathbf{t}} = L_{\mathbf{t}}^{-1} \left( \frac{X_{\mathbf{t}}^\top \mathbf{y}}{n} \right)$ .  $\square$

We use Lemma 1 for proving Theorem 2. For a proof of this lemma, we refer to [28].

**Lemma 1** (Banachiewicz Inversion Formula). *For a block matrix*

$$B = \begin{pmatrix} A_{11} & A_{12} \\ A_{21} & A_{22} \end{pmatrix},$$

*we have:*

(i) *If  $A_{11}$  is nonsingular, then  $B$  is nonsingular if and only if the Schur complement  $S = A_{22} - A_{21}A_{11}^{-1}A_{12}$  is nonsingular.*

(ii) *Furthermore, if both  $A_{11}$  and  $A_{22}$  are nonsingular, then*

$$B^{-1} = \begin{pmatrix} I & -A_{11}^{-1}A_{12}S^{-1} \\ \mathbf{0} & S^{-1} \end{pmatrix} \begin{pmatrix} A_{11}^{-1} & \mathbf{0} \\ -A_{21}A_{11}^{-1} & I \end{pmatrix}.$$

*Proof of Theorem 2.* It is well-known that the inverse of a matrix after a permutation of rows (respectively, columns) is identical to the matrix obtained by applying the same permutation on columns (respectively, rows) on the inverse of the matrix. Therefore without loss of generality we assume that all the zero-elements of  $\mathbf{s} \in \{0, 1\}^p$  appear at the end, in the form:

$$\mathbf{s} = (s_1, \dots, s_m, 0, \dots, 0),$$

where  $m$  indicates the number of non-zeros in  $\mathbf{s}$ . Recall that  $X_{[\mathbf{s}]}$  is the matrix of size  $n \times |\mathbf{s}|$  created by keeping only columns  $j$  of  $X$  for which  $s_j = 1$ . Then, with the notation  $(A)_+$ , defined in Section 6.3,  $L_{\mathbf{s}}$  is given by,

$$\begin{aligned} L_{\mathbf{s}} &= \frac{1}{n} \left[ \begin{pmatrix} (X_{\mathbf{s}}^{\top} X_{\mathbf{s}})_+ & \mathbf{0} \\ \mathbf{0} & \mathbf{0} \end{pmatrix} + \delta \begin{pmatrix} I - (T_{\mathbf{s}}^2)_+ & \mathbf{0} \\ \mathbf{0} & I \end{pmatrix} \right] \\ &= \frac{1}{n} \begin{pmatrix} X_{[\mathbf{s}]}^{\top} X_{[\mathbf{s}]} & \mathbf{0} \\ \mathbf{0} & \delta I \end{pmatrix}, \end{aligned} \quad (21)$$

where we used the fact that for binary vectors  $\mathbf{s}$ ,

$$(X_{\mathbf{s}}^{\top} X_{\mathbf{s}})_+ = X_{[\mathbf{s}]}^{\top} X_{[\mathbf{s}]} \quad \text{and} \quad (T_{\mathbf{s}}^2)_+ = I.$$

From Lemma 1, it is evident that  $L_{\mathbf{t}}$  is invertible if and only if  $X_{[\mathbf{s}]}^{\top} X_{[\mathbf{s}]}$  is invertible. Since  $\widehat{\beta}_{[\mathbf{s}]}$  exists if and only if  $X_{[\mathbf{s}]}^{\top} X_{[\mathbf{s}]}$  is invertible,  $L_{\mathbf{s}}$  is invertible if and only if  $\widehat{\beta}_{[\mathbf{s}]}$  exists. Thus, using Lemma 1, we have

$$\begin{aligned} L_{\mathbf{s}}^{-1} &= n \begin{pmatrix} I & \mathbf{0} \\ \mathbf{0} & \frac{1}{\delta} I \end{pmatrix} \begin{pmatrix} (X_{[\mathbf{s}]}^{\top} X_{[\mathbf{s}]})^{-1} & \mathbf{0} \\ 0 & I \end{pmatrix} \\ &= n \begin{pmatrix} (X_{[\mathbf{s}]}^{\top} X_{[\mathbf{s}]})^{-1} & \mathbf{0} \\ 0 & \frac{1}{\delta} I \end{pmatrix} \end{aligned} \quad (22)$$

To show that  $X_{\mathbf{s}} \widetilde{\beta}_{\mathbf{s}} = X_{[\mathbf{s}]} \widehat{\beta}_{[\mathbf{s}]}$  for  $\mathbf{s} \in \{0, 1\}^p$  where  $X_{[\mathbf{s}]}^{\top} X_{[\mathbf{s}]}$  is invertible, using (22), we obtain

$$L_{\mathbf{s}}^{-1} T_{\mathbf{s}} X^{\top} \mathbf{y} = (X_{[\mathbf{s}]}^{\top} X_{[\mathbf{s}]})^{-1} X_{[\mathbf{s}]}^{\top} \mathbf{y},$$

which guarantees  $X_{[\mathbf{s}]} \widehat{\beta}_{[\mathbf{s}]} = X_{\mathbf{s}} \widetilde{\beta}_{\mathbf{s}}$ . □

We use Lemma 2 for proving Theorem 3. Here, recall that for any vector  $\mathbf{u} \in \mathbb{R}^p$ , the max-norm of  $\mathbf{u}$  is given by

$$\|\mathbf{u}\|_\infty = \max_{j=1,\dots,p} |u_j|.$$

**Lemma 2.** ([3, Theorem 16]) Suppose  $A \in \mathbb{R}^{p \times p}$  is a non-trivial real-valued square matrix with eigenvalues  $\boldsymbol{\eta} = (\eta_1, \dots, \eta_p)^\top$  and  $r$  is a real number such that

$$0 < r < \frac{2}{\|\boldsymbol{\eta}\|_\infty^2}.$$

Then,

$$A^+ = r \sum_{k=0}^{\infty} (I - rA^\top A)^k A^\top.$$

*Proof of Theorem 3.* Consider a point  $\mathbf{t} \in [0, 1]^p$  and a sequence  $\mathbf{t}^{(1)}, \mathbf{t}^{(2)}, \dots \in [0, 1]^p$  converging to  $\mathbf{t}$ . Then  $L_{\mathbf{t}^{(l)}}$  converges to  $L_{\mathbf{t}}$  element-wise as  $l \rightarrow \infty$ . To see this, observe from the definitions of  $L_{\mathbf{t}^{(l)}}$  and  $T_{\mathbf{t}^{(l)}}$  that, with  $Z = \frac{X^\top X}{n} - \frac{\delta}{n}I$ ,

$$L_{\mathbf{t}^{(l)}} = T_{\mathbf{t}^{(l)}} Z T_{\mathbf{t}^{(l)}} + \frac{\delta}{n}I = (T_{\mathbf{t}} - T_{\Delta\mathbf{t}^{(l)}}) Z (T_{\mathbf{t}} - T_{\Delta\mathbf{t}^{(l)}}) + \frac{\delta}{n}I,$$

where  $\Delta\mathbf{t}^{(l)} = \mathbf{t} - \mathbf{t}^{(l)}$ . Expanding the above expression we obtain

$$L_{\mathbf{t}^{(l)}} = L_{\mathbf{t}} - D_i,$$

where the symmetric matrix

$$D_i = T_{\mathbf{t}} Z T_{\Delta\mathbf{t}^{(l)}} + T_{\Delta\mathbf{t}^{(l)}} Z T_{\mathbf{t}} - T_{\Delta\mathbf{t}^{(l)}} Z T_{\Delta\mathbf{t}^{(l)}}.$$

Clearly, element-wise,  $D_i$  is going to  $\mathbf{0}$  as  $i \rightarrow \infty$ . In other words,  $L_{\mathbf{t}^{(l)}}$  converges to  $L_{\mathbf{t}}$  element-wise as  $i \rightarrow \infty$ .

Now suppose that  $\boldsymbol{\eta}_l$  and  $\boldsymbol{\eta}$  are the vector of the eigenvalues of  $L_{\mathbf{t}^{(l)}}$  and  $L_{\mathbf{t}}$ , respectively. Then Proposition 5.2.2 (c) of [2] guarantees the convergence of the eigenvalues of  $L_{\mathbf{t}^{(l)}}$  to that  $L_{\mathbf{t}}$ . Thus,

$$\lim_{l \rightarrow \infty} \|\boldsymbol{\eta}_l\|_\infty = \|\boldsymbol{\eta}\|_\infty.$$

This implies that there exists a large number  $N$  and a constant  $r$  such that

$$0 < r < \frac{2}{\|\boldsymbol{\eta}\|_\infty^2}$$

and

$$0 < r < \frac{2}{\|\boldsymbol{\eta}_l\|_\infty^2}, \quad \text{for all } l \geq N.$$

For such  $r$  and  $N$ , from Lemma 2,

$$L_{\mathbf{t}}^+ = r \sum_{k=0}^{\infty} (I - rL_{\mathbf{t}}^2)^k L_{\mathbf{t}},$$

and

$$L_{\mathbf{t}^{(l)}}^+ = L_{\mathbf{t}^{(l)}}^{-1} = r \sum_{k=0}^{\infty} (I - rL_{\mathbf{t}^{(l)}}^2)^k L_{\mathbf{t}^{(l)}}, \quad \text{for all } l \geq N,$$

where the equality  $L_{\mathbf{t}^{(l)}}^+ = L_{\mathbf{t}^{(l)}}^{-1}$  follows from Theorem 1 since each  $\mathbf{t}^{(l)} \in [0, 1]^p$ . Now observe that

$$L_{\mathbf{t}^{(l)}}^2 = (L_{\mathbf{t}} - D_l)^2 = L_{\mathbf{t}}^2 + G_l,$$

where  $G_l = D_l^2 - D_l L_{\mathbf{t}} - L_{\mathbf{t}} D_l$ , which converges to  $\mathbf{0}$  element-wise as  $l \rightarrow \infty$ . Since

$$L_{\mathbf{t}^{(l)}}^{-1} = r \sum_{k=0}^{\infty} (I - rL_{\mathbf{t}}^2 - rG_l)^k (L_{\mathbf{t}} - D_l), \quad \text{for all } l \geq N,$$

$L_{\mathbf{t}^{(l)}}^{-1}$  converges to  $L_{\mathbf{t}}^+$  element-wise.

As a consequence, since  $X_{\mathbf{t}^{(l)}}$  converges element-wise to  $X_{\mathbf{t}}$ , we can guarantee that

$$\lim_{l \rightarrow \infty} \tilde{\boldsymbol{\beta}}_{\mathbf{t}^{(l)}} = \lim_{l \rightarrow \infty} L_{\mathbf{t}^{(l)}}^{-1} \left( \frac{X_{\mathbf{t}^{(l)}} \mathbf{y}}{n} \right) = \tilde{\boldsymbol{\beta}}_{\mathbf{t}},$$

and thus we trivially have from the definition of  $f_{\lambda}$  that  $\lim_{l \rightarrow \infty} f_{\lambda}(\mathbf{t}^{(l)}) = f_{\lambda}(\mathbf{t})$ .  $\square$

We use Lemma 3, which obtains the partial derivatives of  $\tilde{\boldsymbol{\beta}}_{\mathbf{t}}$  with respect to the elements of  $\mathbf{t}$ , for proving Theorem 4.

**Lemma 3.** For any  $\mathbf{t} \in (0, 1)^p$ , the derivatives of  $\tilde{\boldsymbol{\beta}}_{\mathbf{t}}$  are given by

$$\frac{\partial \tilde{\boldsymbol{\beta}}_{\mathbf{t}}}{\partial t_j} = L_{\mathbf{t}}^{-1} [E_j - E_j Z T_{\mathbf{t}} L_{\mathbf{t}}^{-1} T_{\mathbf{t}} - T_{\mathbf{t}} Z E_{j+1} L_{\mathbf{t}}^{-1} T_{\mathbf{t}}] \left( \frac{X^{\top} \mathbf{y}}{n} \right), \quad j = 1, \dots, p,$$

where

$$Z = \left( \frac{X^{\top} X}{n} - \frac{\delta}{n} I \right),$$

and  $E_j$  is a square matrix of dimension  $p \times p$  with 1 at the  $(j, j)$ -th position and 0 everywhere else.

*Proof.* Existence of  $\tilde{\boldsymbol{\beta}}_{\mathbf{t}}$  for every  $\mathbf{t} \in (0, 1)^p$  and  $\delta > 0$  follows from Theorem 1 which states that  $L_{\mathbf{t}}$  is positive-definite which guarantees the invertibility of  $L_{\mathbf{t}}$ .

Since  $\tilde{\boldsymbol{\beta}}_{\mathbf{t}} = L_{\mathbf{t}}^{-1} T_{\mathbf{t}} \left( \frac{X^{\top} \mathbf{y}}{n} \right)$ , using matrix calculus, for any  $j = 1, \dots, p$ ,

$$\begin{aligned} \frac{\partial \tilde{\boldsymbol{\beta}}_{\mathbf{t}}}{\partial t_j} &= \frac{\partial (L_{\mathbf{t}}^{-1} T_{\mathbf{t}})}{\partial t_j} \left( \frac{X^{\top} \mathbf{y}}{n} \right) \\ &= \left[ \frac{\partial L_{\mathbf{t}}^{-1}}{\partial t_j} T_{\mathbf{t}} + L_{\mathbf{t}}^{-1} \frac{\partial T_{\mathbf{t}}}{\partial t_j} \right] \left( \frac{X^{\top} \mathbf{y}}{n} \right) \\ &= \left[ L_{\mathbf{t}}^{-1} \frac{\partial T_{\mathbf{t}}}{\partial t_j} - L_{\mathbf{t}}^{-1} \frac{\partial L_{\mathbf{t}}}{\partial t_j} L_{\mathbf{t}}^{-1} T_{\mathbf{t}} \right] \left( \frac{X^{\top} \mathbf{y}}{n} \right), \end{aligned}$$

where we used differentiation of an invertible matrix which implies

$$\frac{\partial L_{\mathbf{t}}^{-1}}{\partial t_j} = -L_{\mathbf{t}}^{-1} \frac{\partial L_{\mathbf{t}}}{\partial t_j} L_{\mathbf{t}}^{-1}.$$

Since

$$\frac{\partial T_{\mathbf{t}}}{\partial t_j} = E_j,$$

and the fact that  $L_{\mathbf{t}} = T_{\mathbf{t}} Z T_{\mathbf{t}} + \frac{\delta}{n} I$ , we get

$$\frac{\partial L_{\mathbf{t}}}{\partial t_j} = \frac{\partial T_{\mathbf{t}}}{\partial t_j} Z T_{\mathbf{t}} + T_{\mathbf{t}} Z \frac{\partial T_{\mathbf{t}}}{\partial t_j} = E_j Z T_{\mathbf{t}} + T_{\mathbf{t}} Z E_j.$$

Therefore,

$$\begin{aligned} L_{\mathbf{t}}^{-1} \frac{\partial T_{\mathbf{t}}}{\partial t_j} - L_{\mathbf{t}}^{-1} \frac{\partial L_{\mathbf{t}}}{\partial t_j} L_{\mathbf{t}}^{-1} T_{\mathbf{t}} &= L_{\mathbf{t}}^{-1} E_j - L_{\mathbf{t}}^{-1} E_j Z T_{\mathbf{t}} L_{\mathbf{t}}^{-1} T_{\mathbf{t}} - L_{\mathbf{t}}^{-1} T_{\mathbf{t}} Z E_j L_{\mathbf{t}}^{-1} T_{\mathbf{t}} \\ &= L_{\mathbf{t}}^{-1} [E_j - E_j Z T_{\mathbf{t}} L_{\mathbf{t}}^{-1} T_{\mathbf{t}} - T_{\mathbf{t}} Z E_j L_{\mathbf{t}}^{-1} T_{\mathbf{t}}]. \end{aligned}$$

This completes the proof Lemma 3.  $\square$

*Proof of Theorem 4.* To obtain the gradient  $\nabla f_{\lambda}(\mathbf{t})$  for  $\mathbf{t} \in (0, 1)^p$ , let  $\gamma_{\mathbf{t}} = T_{\mathbf{t}} \tilde{\beta}_{\mathbf{t}} = \mathbf{t} \odot \tilde{\beta}$ . Then,

$$\begin{aligned} \|\mathbf{y} - X_{\mathbf{t}} \tilde{\beta}_{\mathbf{t}}\|_2^2 &= \|\mathbf{y} - X \gamma_{\mathbf{t}}\|_2^2 \\ &= (\mathbf{y} - X \gamma_{\mathbf{t}})^{\top} (\mathbf{y} - X \gamma_{\mathbf{t}}) \\ &= \mathbf{y}^{\top} \mathbf{y} - 2 \gamma_{\mathbf{t}}^{\top} (X^{\top} \mathbf{y}) + \gamma_{\mathbf{t}}^{\top} (X^{\top} X) \gamma_{\mathbf{t}}. \end{aligned} \quad (23)$$

Consequently,

$$\begin{aligned} \frac{\partial f_{\lambda}(\mathbf{t})}{\partial t_j} &= \frac{1}{n} \frac{\partial}{\partial t_j} [\|\mathbf{y} - X_{\mathbf{t}} \tilde{\beta}_{\mathbf{t}}\|_2^2] + \lambda \\ &= -\frac{2}{n} \left( \frac{\partial \gamma_{\mathbf{t}}}{\partial t_j} \right)^{\top} (X^{\top} \mathbf{y}) + \frac{2}{n} \left( \frac{\partial \gamma_{\mathbf{t}}}{\partial t_j} \right)^{\top} (X^{\top} X) \gamma_{\mathbf{t}} + \lambda \\ &= \frac{2}{n} \left( \frac{\partial \gamma_{\mathbf{t}}}{\partial t_j} \right)^{\top} [(X^{\top} X) \gamma_{\mathbf{t}} - (X^{\top} \mathbf{y})] + \lambda \\ &= 2 \left( \frac{\partial \gamma_{\mathbf{t}}}{\partial t_j} \right)^{\top} \mathbf{a}_{\mathbf{t}} + \lambda, \end{aligned} \quad (24)$$

where

$$\mathbf{a}_{\mathbf{t}} = \left( \frac{X^{\top} X}{n} \right) \gamma_{\mathbf{t}} - \left( \frac{X^{\top} \mathbf{y}}{n} \right).$$

From the definition of  $\tilde{\beta}_{\mathbf{t}}$  and  $\gamma_{\mathbf{t}}$ ,

$$\begin{aligned} \frac{\partial \gamma_{\mathbf{t}}}{\partial t_j} &= \frac{\partial T_{\mathbf{t}} \tilde{\beta}_{\mathbf{t}}}{\partial t_j} \\ &= \frac{\partial T_{\mathbf{t}}}{\partial t_j} \tilde{\beta}_{\mathbf{t}} + T_{\mathbf{t}} \frac{\partial \tilde{\beta}_{\mathbf{t}}}{\partial t_j} \\ &= E_j \tilde{\beta}_{\mathbf{t}} + T_{\mathbf{t}} L_{\mathbf{t}}^{-1} [E_j - E_j Z T_{\mathbf{t}} L_{\mathbf{t}}^{-1} T_{\mathbf{t}} - T_{\mathbf{t}} Z E_j L_{\mathbf{t}}^{-1} T_{\mathbf{t}}] \left( \frac{X^{\top} \mathbf{y}}{n} \right), \end{aligned}$$

where the last equality is obtained using Lemma 3 and the fact that  $\frac{\partial T_t}{\partial t_j} = E_j$  and  $Z = \left( \frac{X^\top X}{n} - \frac{\delta}{n} I \right)$ .

Further simplification yields

$$\begin{aligned} \frac{\partial \gamma_t}{\partial t_j} &= E_j \tilde{\beta}_t + T_t L_t^{-1} \left[ E_j \left( \frac{X^\top \mathbf{y}}{n} \right) - E_j Z \gamma_t - T_t Z E_j \tilde{\beta}_t \right] \\ &= E_j \tilde{\beta}_t - T_t L_t^{-1} E_j \mathbf{b}_t - T_t L_t^{-1} T_t Z E_j \tilde{\beta}_t, \end{aligned} \quad (25)$$

and we recall that

$$\mathbf{b}_t = Z \gamma_t - \left( \frac{X^\top \mathbf{y}}{n} \right) = \mathbf{a}_t - \frac{\delta}{n} \gamma_t.$$

For a further simplification, recall that

$$\mathbf{c}_t = L_t^{-1} (\mathbf{t} \odot \mathbf{a}_t),$$

and

$$\mathbf{d}_t = Z (\mathbf{t} \odot \mathbf{c}_t).$$

Then, from (25), the matrix  $\frac{\partial \gamma_t}{\partial \mathbf{t}}$  of dimension  $p \times p$  with  $j$ -th column being  $\frac{\partial \gamma_t}{\partial t_j}$  can be expressed as

$$\frac{\partial \gamma_t}{\partial \mathbf{t}} = \text{Diag}(\tilde{\beta}_t) - T_t L_t^{-1} \text{Diag}(\mathbf{b}_t) - T_t L_t^{-1} T_t Z \text{Diag}(\tilde{\beta}_t). \quad (26)$$

From (24), with  $\mathbf{1}$  representing a vector of all ones,  $\nabla f_\lambda(\mathbf{t})$  can be expressed as

$$\begin{aligned} \nabla f_\lambda(\mathbf{t}) &= 2 \text{Diag}(\tilde{\beta}_t) \mathbf{a}_t - 2 \text{Diag}(\mathbf{b}_t) L_t^{-1} T_t \mathbf{a}_t - 2 \text{Diag}(\tilde{\beta}_t) Z T_t L_t^{-1} T_t \mathbf{a}_t + \lambda \mathbf{1} \\ &= 2 (\tilde{\beta}_t \odot \mathbf{a}_t) - 2 \text{Diag}(\mathbf{b}_t) \mathbf{c}_t - 2 \text{Diag}(\tilde{\beta}_t) Z T_t \mathbf{c}_t + \lambda \mathbf{1} \\ &= 2 (\tilde{\beta}_t \odot \mathbf{a}_t) - 2 (\mathbf{b}_t \odot \mathbf{c}_t) - 2 (\tilde{\beta}_t \odot \mathbf{d}_t) + \lambda \mathbf{1} \\ &= 2 (\tilde{\beta}_t \odot (\mathbf{a}_t - \mathbf{d}_t)) - 2 (\mathbf{b}_t \odot \mathbf{c}_t) + \lambda \mathbf{1} \\ &= \zeta_t + \lambda \mathbf{1}, \end{aligned}$$

where

$$\zeta_t = 2 (\tilde{\beta}_t \odot (\mathbf{a}_t - \mathbf{d}_t)) - 2 (\mathbf{b}_t \odot \mathbf{c}_t).$$

To solve the optimization problem (14) using any gradient based method, we need to compute the gradients of  $g_\lambda(\mathbf{w})$ :

$$\nabla g_\lambda(\mathbf{w}) = \left( \frac{\partial g_\lambda(\mathbf{w})}{\partial w_1}, \dots, \frac{\partial g_\lambda(\mathbf{w})}{\partial w_p} \right)^\top.$$

Recall that we define  $g_\lambda(\mathbf{w}) = f_\lambda(\mathbf{t}(\mathbf{w}))$  in (13) and

$$f_\lambda(\mathbf{t}) = \frac{1}{n} \|\mathbf{y} - X_t \tilde{\beta}_t\|_2^2 + \lambda \sum_{j=1}^p t_j.$$

Then, from the chain rule of differentiation, for each  $j = 1, \dots, p$ ,

$$\frac{\partial g_\lambda(\mathbf{w})}{\partial w_j} = \frac{\partial f_\lambda(\mathbf{t})}{\partial t_j} (2w_j \exp(-w_j^2)).$$

Alternatively, in short,

$$\nabla g_\lambda(\mathbf{w}) = \nabla f_\lambda(\mathbf{t}) \odot (2\mathbf{w} \odot \exp(-\mathbf{w} \odot \mathbf{w})). \quad (27)$$

□

*Proof of Proposition 1.* From Theorem 4, we obtain  $\nabla f_\lambda(\mathbf{t})$  as follows,

$$\nabla f_\lambda(\mathbf{t}) = \zeta_{\mathbf{t}} + \lambda \mathbf{1},$$

where  $\zeta_{\mathbf{t}} \in \mathbb{R}^p$  (recalling from Theorem 4) is given by

$$\zeta_{\mathbf{t}} = 2 \left( \tilde{\beta}_{\mathbf{t}} \odot (\mathbf{a}_{\mathbf{t}} - \mathbf{d}_{\mathbf{t}}) \right) - 2 (\mathbf{b}_{\mathbf{t}} \odot \mathbf{c}_{\mathbf{t}}), \quad (28)$$

with

$$\begin{aligned} \mathbf{a}_{\mathbf{t}} &= \left( \frac{X^\top X}{n} \right) (\mathbf{t} \odot \tilde{\beta}_{\mathbf{t}}) - \left( \frac{X^\top \mathbf{y}}{n} \right), \\ \mathbf{b}_{\mathbf{t}} &= \mathbf{a}_{\mathbf{t}} - \frac{\delta}{n} (\mathbf{t} \odot \tilde{\beta}_{\mathbf{t}}), \\ \mathbf{c}_{\mathbf{t}} &= L_{\mathbf{t}}^{-1} (\mathbf{t} \odot \mathbf{a}_{\mathbf{t}}), \quad \text{and} \\ \mathbf{d}_{\mathbf{t}} &= \left( \frac{X^\top X}{n} - \frac{\delta}{n} I \right) (\mathbf{t} \odot \mathbf{c}_{\mathbf{t}}). \end{aligned}$$

From the definition of  $\tilde{\beta}_{\mathbf{t}}$ , it is easy to show that for any  $j$ , if we fix  $t_i$  for all  $i \neq j$ , then the  $j$ -th component of  $\tilde{\beta}_{\mathbf{t}}$  goes to zero as  $t_j \downarrow 0$ , that is,  $\lim_{t_j \downarrow 0} \tilde{\beta}_{\mathbf{t}}(j) = 0$ . Similarly,  $\lim_{t_j \downarrow 0} \mathbf{c}_{\mathbf{t}}(j) = 0$ . Therefore, from the expression of  $\zeta_{\mathbf{t}}$  in (28), we have  $\lim_{t_j \downarrow 0} \zeta_{\mathbf{t}}(j) = 0$ . □

We need Lemma 4 for proving Theorem 5; we refer to [30] for a proof of Lemma 4.

**Lemma 4** (Woodbury matrix identity or Duncan Inversion Formula). *For any conformable matrices  $A, B_1$ , and  $B_2$ , and  $C$ ,*

$$(A + B_1 C B_2)^{-1} = A^{-1} - A^{-1} B_1 (C^{-1} + B_2 A^{-1} B_1)^{-1} B_2 A^{-1}.$$

*Proof of Theorem 5.* Now recall the expression of  $L_{\mathbf{t}}$  from (6):

$$L_{\mathbf{t}} = \frac{1}{n} \left[ X_{\mathbf{t}}^\top X_{\mathbf{t}} + \delta (I - T_{\mathbf{t}}^2) \right].$$

Since the gradient descent algorithm in COMBSS computes  $g_\lambda(\mathbf{w})$  for  $\mathbf{w} \in \mathbb{R}^p$ , from the map  $\mathbf{w} \mapsto \mathbf{t}(\mathbf{w})$ , we care about solving  $L_{\mathbf{t}} \mathbf{z} = \mathbf{u}$  only for  $\mathbf{t} \in [0, 1]^p$ . For such a  $\mathbf{t}$ ,

$$S_{\mathbf{t}} := \frac{n}{\delta} (I - T_{\mathbf{t}}^2)^{-1}$$

exists. In particular,  $S_{\mathbf{t}}$  is a  $p$ -dimensional diagonal matrix with the diagonal elements given by  $(n/\delta(1-t_1^2), \dots, n/\delta(1-t_p^2))$ , which is easy to compute. Further, if we take

$$A = \frac{\delta}{n} (I - T_{\mathbf{t}}^2), \quad B_1 = B_2^{\top} = \frac{1}{\sqrt{n}} X_{\mathbf{t}}^{\top}, \quad \text{and} \quad C = I$$

in Lemma 4, then,

$$L_{\mathbf{t}}^{-1} = S_{\mathbf{t}} - \frac{1}{n} S_{\mathbf{t}} X_{\mathbf{t}}^{\top} \left( I + \frac{1}{n} X_{\mathbf{t}} S_{\mathbf{t}} X_{\mathbf{t}}^{\top} \right)^{-1} X_{\mathbf{t}} S_{\mathbf{t}}.$$

Since  $S_{\mathbf{t}}$  is diagonal matrix, it is easy to see that

$$\tilde{L}_{\mathbf{t}} := I + \frac{1}{n} X_{\mathbf{t}} S_{\mathbf{t}} X_{\mathbf{t}}^{\top}$$

is a symmetric positive definite matrix of dimension  $n \times n$  (in comparison,  $L_{\mathbf{t}}$  is of dimension  $p \times p$ ). Thus,  $\tilde{L}_{\mathbf{t}}^{-1}$  exists and

$$L_{\mathbf{t}}^{-1} \mathbf{u} = (S_{\mathbf{t}} \mathbf{u}) - \frac{1}{n} S_{\mathbf{t}} X_{\mathbf{t}}^{\top} \tilde{L}_{\mathbf{t}}^{-1} (X_{\mathbf{t}} S_{\mathbf{t}} \mathbf{u}).$$

□

*Proof of Theorem 6.* For the same reasons mentioned in the proof of Theorem 2, without loss of generality we can assume that all the zero elements of  $\mathbf{t}$  appear at the end of  $\mathbf{t}$ ; that is,  $\mathbf{t}$  is of the form:

$$\mathbf{t} = (t_1, \dots, t_m, 0, \dots, 0),$$

where  $m$  indicates the number of non-zero elements in  $\mathbf{t}$ . Then,  $L_{\mathbf{t}}$  is given by

$$\begin{aligned} L_{\mathbf{t}} &= \frac{1}{n} \left[ \begin{pmatrix} (X_{\mathbf{t}}^{\top} X_{\mathbf{t}})_{+} & \mathbf{0} \\ \mathbf{0} & \mathbf{0} \end{pmatrix} + \delta \begin{pmatrix} I - (T_{\mathbf{t}}^2)_{+} & \mathbf{0} \\ \mathbf{0} & I \end{pmatrix} \right] \\ &= \begin{pmatrix} (L_{\mathbf{t}})_{+} & \mathbf{0} \\ \mathbf{0} & \frac{\delta}{n} I \end{pmatrix}. \end{aligned} \tag{29}$$

Since  $\mathbf{t} \in [0, 1]^p$ , from Theorem 1,  $L_{\mathbf{t}}$  is a positive definite matrix. It is a well-known fact that every principle submatrix of a positive definite matrix is also positive definite. Thus,  $(L_{\mathbf{t}})_{+}$  is positive definite and hence invertible. Using Lemma 1,

$$\begin{aligned} L_{\mathbf{t}}^{-1} &= \begin{pmatrix} ((L_{\mathbf{t}})_{+})^{-1} & \mathbf{0} \\ \mathbf{0} & I \end{pmatrix} \begin{pmatrix} I & \mathbf{0} \\ \mathbf{0} & \frac{n}{\delta} I \end{pmatrix} \\ &= \begin{pmatrix} ((L_{\mathbf{t}})_{+})^{-1} & \mathbf{0} \\ \mathbf{0} & \frac{n}{\delta} I \end{pmatrix}. \end{aligned} \tag{30}$$

This completes the proof of (i).

Now observe that

$$\begin{pmatrix} \frac{X_{\mathbf{t}}^{\top} \mathbf{y}}{n} \\ \mathbf{0} \end{pmatrix} = \begin{pmatrix} \left( \frac{X_{\mathbf{t}}^{\top} \mathbf{y}}{n} \right)_{+} \\ \mathbf{0} \end{pmatrix} = \begin{pmatrix} (\mathbf{t})_{+} \odot \left( \frac{X_{\mathbf{t}}^{\top} \mathbf{y}}{n} \right)_{+} \\ \mathbf{0} \end{pmatrix}.$$

Since  $\tilde{\beta}_{\mathbf{t}} = L_{\mathbf{t}}^{-1} \begin{pmatrix} \frac{X_{\mathbf{t}}^{\top} \mathbf{y}}{n} \\ \mathbf{0} \end{pmatrix}$ , using (30), we complete the proof of (ii). Similar arguments prove (iii); hence for conciseness that proof is omitted here. □

## B Gradient Descent Methods

In this section, we review two popular gradient descent methods, namely, the basic gradient descent method and the Adam optimizer. In each iteration, the basic gradient descent method uses only the current gradient for finding the descent direction  $\Delta \mathbf{w}$ . On the other hand, the Adam optimizer uses the current as well as all the past gradients for finding  $\Delta \mathbf{w}$ , in such a way that the algorithm moves with *momentum* that can provide acceleration and can help in bypassing saddle points and local minima of the objective function. See, for example, [18], for more details on gradient descent methods.

### B.1 Basic Gradient Descent Method

For each iteration  $l = 1, 2, \dots$ , let  $\mathbf{w}^{(l-1)}$  be the value of  $\mathbf{w}$  obtained from the previous iteration; here, the first iteration starts with the initial vector  $\mathbf{w}^{(0)}$  given to the algorithm. Then, the next point is obtained from the update:

$$\mathbf{w}^{(l)} = \mathbf{w}^{(l-1)} - \alpha \nabla g_\lambda(\mathbf{w}^{(l-1)}),$$

for a positive constant  $\alpha$  known as learning rate. That means, the descent step  $\Delta \mathbf{w}$  in the  $l$ -th iteration is  $-\alpha \nabla g_\lambda(\mathbf{w}^{(l-1)})$ , which is in the negative gradient direction, i.e., the most rapid decreasing direction. The learning parameter  $\alpha$  controls the convergence rate: smaller  $\alpha$  would slow convergence and larger  $\alpha$  would lead to divergence. To overcome the difficulty of selecting the learning parameter and increase the convergence speed, there are several methods proposed in the existing literature; among them, most popular one is the Adam optimizer, which is presented below.

### B.2 The Adam Optimizer

The Adam (short for Adaptive Moment Estimation) optimizer [17] uses the following exponential smoothing of the gradients and the squared gradients of the objective function  $g_\lambda(\mathbf{w})$ . For each iteration  $l = 1, 2, \dots$ , with  $\mathbf{w}^{(l-1)}$  being the value of  $\mathbf{w}$  obtained from the previous iteration, let

$$\begin{aligned} \mathbf{u}^{(l)} &= -(1 - \xi_1) \sum_{k=0}^{l-1} \xi_1^{l-k-1} \nabla g_\lambda(\mathbf{w}^{(k)}), \quad (\text{momentum update}) \\ \mathbf{v}^{(l)} &= (1 - \xi_2) \sum_{k=0}^{l-1} \xi_2^{l-k-1} \left( \nabla g_\lambda(\mathbf{w}^{(k)}) \odot \nabla g_\lambda(\mathbf{w}^{(k)}) \right), \end{aligned}$$

with  $\mathbf{u}^{(0)} = \mathbf{v}^{(0)} = \mathbf{0}$  and  $\xi_1, \xi_2 \in [0, 1)$ . The default choices are  $\xi_1 = 0.9$  and  $\xi_2 = 0.999$ . Further take,

$$\hat{\mathbf{u}}^{(l)} = \frac{\mathbf{u}^{(l)}}{(1 - \xi_1^l)} \quad \text{and} \quad \hat{\mathbf{v}}^{(l)} = \frac{\mathbf{v}^{(l)}}{(1 - \xi_2^l)}.$$

Finally, the  $\mathbf{w}$  vector is updated using

$$\mathbf{w}^{(l)} = \mathbf{w}^{(l-1)} + \alpha \frac{\hat{\mathbf{u}}^{(l)}}{\sqrt{\hat{\mathbf{v}}^{(l)} + c}}, \quad l = 1, 2, \dots,$$

where the division, multiplication and addition are element-wise, and  $c$  is a constant of order  $1 \times 10^{-8}$  to avoid division by zero and  $\alpha$  is a positive constant. This means, the descent step  $\Delta \mathbf{w}$  in the  $l$ -th iteration is  $\alpha \mathbf{u}^{(l)} / \sqrt{\mathbf{v}^{(l)}} + c$ , which depends on all the gradients computed up to the  $l$ -th iteration.

Observe that the updates  $\mathbf{u}$  and  $\mathbf{v}$  can be rewritten as the following easy to implement recursive expressions:

$$\begin{aligned} \mathbf{u}^{(l)} &= \xi_1 \mathbf{u}^{(l-1)} - (1 - \xi_1) \nabla g_\lambda(\mathbf{w}^{(l-1)}), \\ \mathbf{v}^{(l)} &= \xi_2 \mathbf{v}^{(l-1)} + (1 - \xi_2) \left( \nabla g_\lambda(\mathbf{w}^{(l-1)}) \odot \nabla g_\lambda(\mathbf{w}^{(l-1)}) \right). \end{aligned} \quad (31)$$

## C Additional Simulation Results

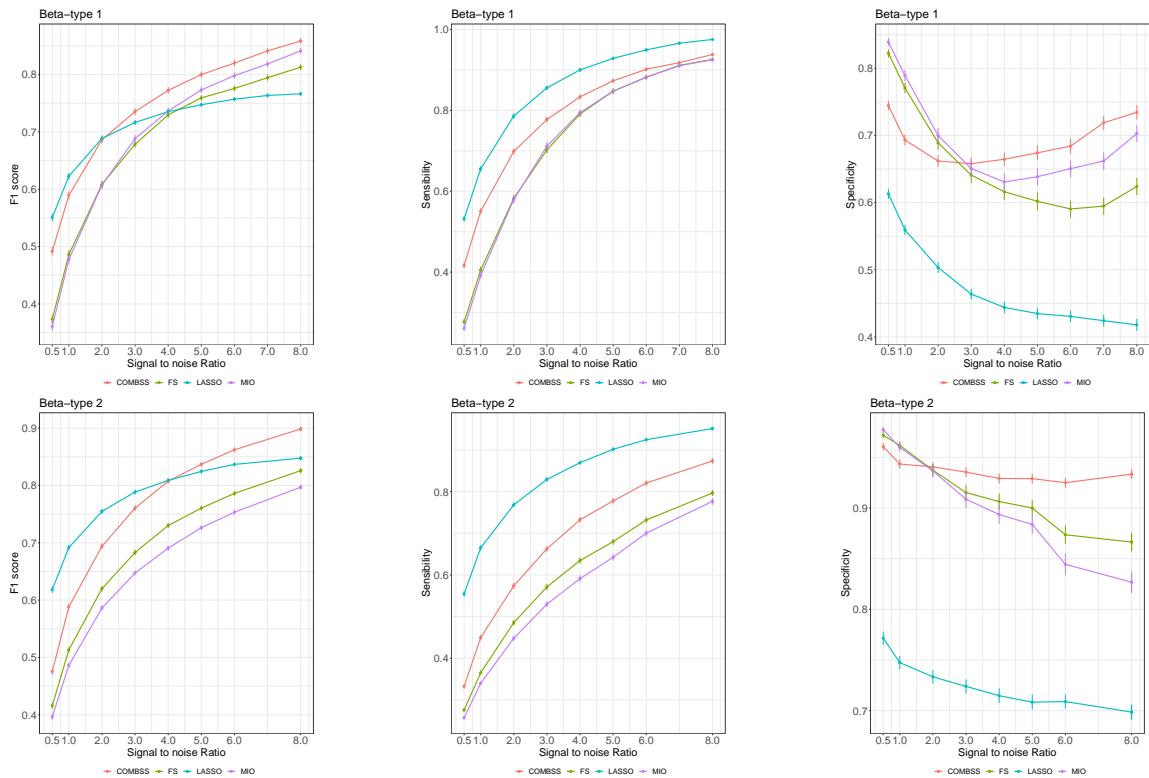


Figure 11: Performance results in terms of F1-score, Sensibility, and Specificity, for the low-dimensional cases:  $n = 100$ ,  $p = 20$ ,  $\rho = 0.8$ , true active predictor is 10 with Beta-type 1 (top plots) and Beta-type 2 (bottom plots).

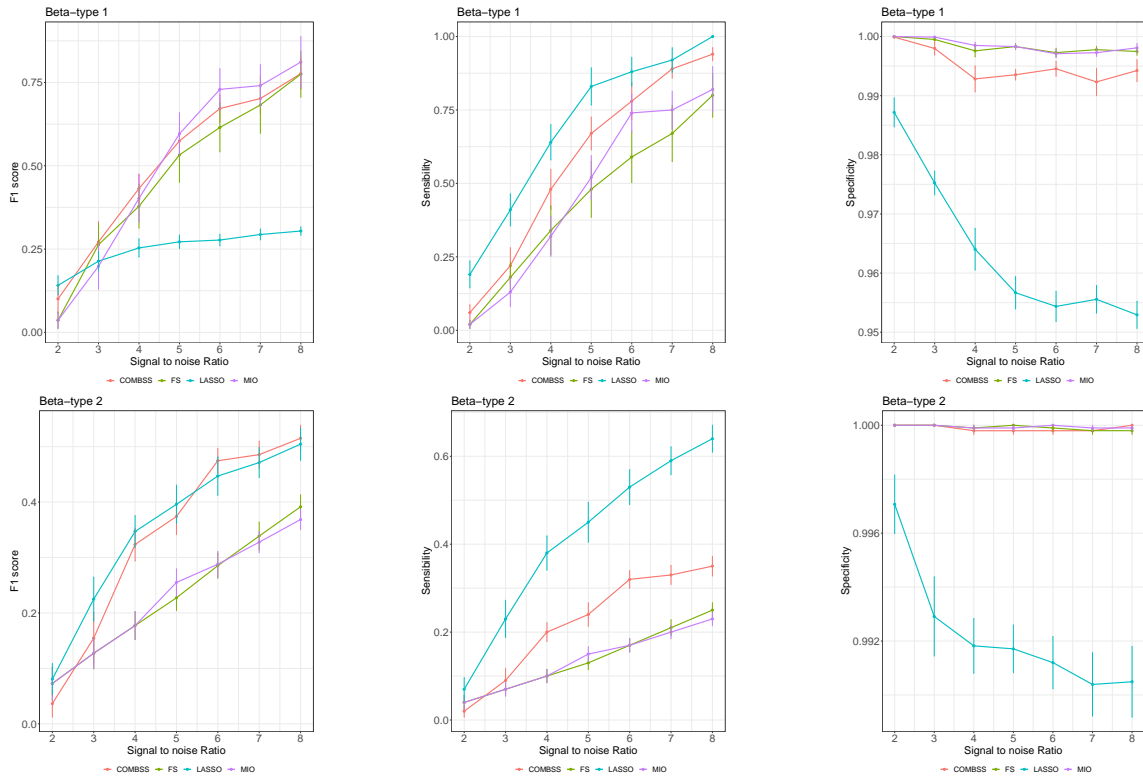


Figure 12: Performance results in terms of F1-score, Sensibility, and Specificity, for the high-dimensional cases:  $n = 100$ ,  $p = 1000$ ,  $\rho = 0.8$ , true active predictor is 10 with Beta-type 1 (top plots) and Beta-type 2 (bottom plots).

## References

- [1] H. Akaike. Information theory and an extension of the maximum likelihood principle. In *Second International Symposium on Information Theory (Tsahkadsor, 1971)*, pages 267–281. 1973.
- [2] M. Artin. *Algebra*. Pearson Prentice Hall, 2011.
- [3] A. Ben-Israel and A. Charnes. Contributions to the theory of generalized inverses. *J. Soc. Indust. Appl. Math.*, 11:667–699, 1963.
- [4] D. Bertsimas, A. King, and R. Mazumder. Best subset selection via a modern optimization lens. *The Annals of Statistics*, 44(2):813 – 852, 2016.
- [5] J. Chen and Z. Chen. Extended Bayesian information criteria for model selection with large model spaces. *Biometrika*, 95(3):759–771, 2008.
- [6] D. Chicco and G. Jurman. The advantages of the matthews correlation coefficient (mcc) over f1 score and accuracy in binary classification evaluation. *BMC genomics*, 21(1):1–13, 2020.
- [7] M. A. Efroymson. Stepwise regression—a backward and forward look. *Presented at the Eastern Regional Meetings of the Institute of Mathematical Statistics, Florham Park, New Jersey*, 1966.

- [8] J. Fan and R. Li. Statistical challenges with high dimensionality: feature selection in knowledge discovery. In *International Congress of Mathematicians. Vol. III*, pages 595–622. Eur. Math. Soc., Zürich, 2006.
- [9] J. Fan and J. Lv. A selective overview of variable selection in high dimensional feature space. *Statist. Sinica*, 20(1):101–148, 2010.
- [10] G. M. Furnival and R. W. Wilson. Regressions by leaps and bounds. *Technometrics*, 42:69–79, 2000.
- [11] G. H. Golub and C. F. Van Loan. *Matrix computations*. Johns Hopkins Studies in the Mathematical Sciences. Johns Hopkins University Press, Baltimore, MD, third edition, 1996.
- [12] Gurobi Optimization, LLC. Gurobi Optimizer Reference Manual, 2022.
- [13] T. Hastie, R. Tibshirani, and R. Tibshirani. *bestsubset: Tools for best subset selection in regression*, 2018. R package version 1.0.10.
- [14] T. Hastie, R. Tibshirani, and R. Tibshirani. Best subset, forward stepwise or lasso? analysis and recommendations based on extensive comparisons. *Statistical Science*, 35(4):579–592, 2020.
- [15] H. Hazimeh and R. Mazumder. Fast best subset selection: coordinate descent and local combinatorial optimization algorithms. *Oper. Res.*, 68(5):1517–1537, 2020.
- [16] R. R. Hocking and R. N. Leslie. Selection of the best subset in regression analysis. *Technometrics*, 9:531–540, 1967.
- [17] D. P. Kingma and J. Ba. Adam: A method for stochastic optimization. In Y. Bengio and Y. LeCun, editors, *3rd International Conference on Learning Representations, ICLR 2015, San Diego, CA, USA, May 7-9, 2015, Conference Track Proceedings*, 2015.
- [18] M. J. Kochenderfer and T. A. Wheeler. *Algorithms for optimization*. MIT Press, Cambridge, MA, 2019.
- [19] T. Lumley. *leaps: Regression Subset Selection*, 2020. R package version 3.1, based on Fortran code by Alan Miller.
- [20] N. Meinshausen. Relaxed Lasso. *Comput. Statist. Data Anal.*, 52(1):374–393, 2007.
- [21] A. Miller. *Subset selection in regression*, volume 95 of *Monographs on Statistics and Applied Probability*. Chapman & Hall/CRC, Boca Raton, FL, 2019.
- [22] S. Müller and A. H. Welsh. On model selection curves. *Intl. Statist. Reviews*, 78(2):240–256, 2010.
- [23] B. K. Natarajan. Sparse approximate solutions to linear systems. *SIAM J. Comput.*, 24(2):227–234, 1995.
- [24] G. Schwarz. Estimating the dimension of a model. *Ann. Statist.*, 6(2):461–464, 1978.
- [25] W. Su, M. g. Bogdan, and E. Candès. False discoveries occur early on the Lasso path. *Ann. Statist.*, 45(5):2133–2150, 2017.

- [26] Y. Takano and R. Miyashiro. Best subset selection via cross-validation criterion. *TOP*, 28:475–488, 2020.
- [27] G. Tarr, S. Muller, and A. H. Welsh. mplot: An r package for graphical model stability and variable selection procedures. *J. Statist. Software*, 83(9):1–28, 2018.
- [28] Y. Tian and Y. Takane. Schur complements and Banachiewicz-Schur forms. *Electron. J. Linear Algebra*, 13:405–418, 2005.
- [29] R. Tibshirani. Regression shrinkage and selection via the lasso. *J. Roy. Statist. Soc. Ser. B*, 58(1):267–288, 1996.
- [30] M. A. Woodbury. *Inverting modified matrices*. Princeton University, Princeton, N. J., 1950. Statistical Research Group, Memo. Rep. no. 42,.
- [31] J. Zhu, C. Wen, J. Zhu, H. Zhang, and X. Wang. A polynomial algorithm for best-subset selection problem. *Proc. Natl. Acad. Sci. USA*, 117(52):33117–33123, 2020.